Thornton Tomasetti

Arecibo Telescope Collapse

Forensic Investigation

Thornton Tomasetti **NN20209**

Prepared For

Arecibo Observatory, operated by **Florida Space Institute**, **University of Central Florida** under cooperative agreement with the **National Science Foundation**

Prepared By

John Abruzzo, P.E., S.E.
Liling Cao, Ph.D., P.E.
Pierre Ghisbain, Ph.D., P.E.

Thornton Tomasetti, Inc.
120 Broadway
New York, NY 10271
+1.212.367.3000
www.ThorntonTomasetti.com

July 25, 2022

Preface

After a first cable failed on the Arecibo Telescope on August 10, 2020, we (Thornton Tomasetti) were engaged by the University of Central Florida (UCF) to be the Engineer of Record for the necessary repairs to stabilize the structure. As preparations were being made for the repairs, a second cable failed on November 6, 2020. On November 19, 2020, the National Science Foundation (NSF) adopted our recommendation to decommission the telescope. The telescope collapsed on its own when additional cables failed on December 1, 2020. We were subsequently retained to perform a forensic investigation of the cable failures and telescope collapse.

We performed the investigation in collaboration with Socotec (formerly Lucius Pitkin), who analyzed and tested samples of the telescope's cables and socket connections in their Brooklyn, NY laboratory. We also worked with Socotec and Lehigh University's Fritz Laboratory to perform a full-scale load test of one of the sockets. Neutron radiography of some of the sockets was performed by Dr. Adrian Brügger of Columbia University in collaboration with the Oak Ridge National Laboratory. Langan provided geotechnical consulting services to support our analysis of the telescope's response to earthquakes.

Before the collapse, UCF retained Wiss, Janney, Elstner Associates (WJE) to investigate the first cable failure and inform the repair plan. The socket connection and matching cable end where the first failure occurred were analyzed by WJE in collaboration with the NASA Engineering and Safety Center (NESC). We reviewed WJE's report,[1] which includes the NESC report, and used some of the reported results as additional data to support our investigation.

Unless otherwise noted, the figures in this report and attached appendices were produced by Thornton Tomasetti on behalf of NSF.

[1] Wiss, Janney, Elstner Associates (WJE). *Auxiliary Main Cable Socket Failure Investigation.* June 21, 2021. Draft report provided by WJE.

Executive Summary

Completed in 1963, the Arecibo Telescope was the largest radio telescope in the world until 2016. The radio feeds of the telescope were located on a steel platform weighing approximately 1.8 million pounds and suspended 500 feet above ground from three concrete towers with more than four miles of steel cables. The cables were arranged in parallel clusters of four or five from tower top to platform and tower top to ground respectively. The telescope was modified in the 1990s to allow the installation of the Gregorian dome and accommodate the increased weight of the platform. At that time, additional cables were installed as single elements from platform to tower to ground. Each cable was a single strand comprising more than 100 high-strength steel wires arranged in concentric layers around a core.

The telescope collapsed on December 1, 2020, after the progressive failure of support cables over a four-month period. The cable failures leading to the collapse occurred at cable ends, where cables are connected to supports with zinc-filled spelter sockets. A first and second socket failed on August 10 and November 6, 2020, respectively, and a third socket failure triggered the collapse on December 1, 2020. All of these failures occurred during fair weather and under normal environmental conditions.

Between February 2021 and May 2022, we investigated the collapse by recovering and testing samples of the cables and sockets, reviewing design documents and maintenance records, and performing a variety of analyses. Our investigation considered the entirety of the telescope's structure, with a particular focus on the cable sockets since they were ultimately the structure's weak point.

We first reviewed the structural design documents for the original construction of the telescope completed in 1963 and the two major upgrades completed in 1974 and 1997. By design, the forces in the cable system were on the higher end of what is typically seen in cable-supported structures, although the expected capacities were still twice those forces. While the telescope was designed to resist loads from hurricanes, it was already highly stressed under its own weight.

We also reviewed the structural inspection and maintenance records produced over the 57 years of the telescope's life. Although the structure was generally well maintained, several conditions were observed on the cable system over time, such as paint degradation, moisture intrusion, vibrations, and individual wire breaks. These conditions were generally addressed adequately and did not significantly contribute to the collapse. In a 2003 inspection, the telescope's Engineer of Record observed that cables had slipped out of their sockets by as much as one-half of an inch and attributed the slips to have occurred during the fabrication or testing of the cables. A later report in 2011 noted that the cable slips remained unchanged from 2003. To our knowledge, the Observatory staff was not instructed to monitor cable slips, nor were they provided with a limit on acceptable cable slip. After Hurricane Maria in 2017, the Observatory staff observed and recorded cable slips of more than one inch on two of the sockets. There is no documentation to show whether these cable slips increased during the hurricane, and to our knowledge they were not identified as an immediate structural integrity issue.

We performed a laboratory analysis of cable and socket samples recovered from the collapsed structure. The results confirm that the cable system met the design specifications on material strength and composition, and was in good condition. We reviewed the analysis performed by Wiss, Janney, Elstner

Associates (WJE) and the NASA Engineering and Safety Center (NESC) of the first socket that failed,[2] and dissected five additional sockets including the second socket that failed and the socket exhibiting the largest cable slip. In the failed and distressed sockets, the zinc casting that holds the cable in the socket experienced significant material flow, allowing the cable to slip. The zinc's mechanical properties showed considerable variability between sockets and within each socket.

We performed an analysis of the telescope structure to determine the forces in the cable system under various conditions, including normal telescope operation and extreme environmental events such as windstorms and earthquakes. The results confirm that the cable system was highly stressed under its own weight, with cable tensions generally consistent with the design documents. Two recent extreme events – Hurricane Maria in 2017 and the January 2020 earthquake sequence – were specifically analyzed and estimated to have temporarily increased the cable tensions by up to 15 percent. This increase could have exacerbated the cable slip in some of the sockets. We analyzed the impact of the first two cable failures on the remaining cables. The first cable to fail was installed in the 1990s and, since it was an isolated cable, its tension could not be redistributed to adjacent parallel cables. Instead, the first cable failure impacted the cable tensions throughout the structure and resulted in a rotation of the telescope's platform.

We studied the sockets to determine why and how some of the sockets exhibited large cable slips and failed while other sockets of identical design and loaded with comparable cable tensions did not. The socket strength analysis involved calculations, finite element analysis, and a full-scale load test to failure. The analysis concludes that the long-term strength of a socket depends on how the cable wires are splayed out in the zinc during socketing. Zinc slowly flows under shear stress when the splayed-out wires, which are typically the two outer layers of the cable, cannot alone resist the cable tension. This condition exists when the wires are insufficiently splayed out for the given cable tension. In this condition, the socket is bound to fail because the zinc will continue to flow until the cable pulls out of the socket entirely. The failure will occur after some time depending on the cable tension and the splayed-out wire geometry, and will be preceded by visible cable slip. Proof-loading of the cable by loading over a period of minutes or hours is not sufficient to assure long-term adequacy of sockets.

From the above reviews and analyses, our investigation concludes that the progressive cable failures and eventual collapse of the Arecibo Telescope were caused by a combination of five factors: (1) the manual and inconsistent splay of the wires during cable socketing, (2) the design of the cable system with relatively low safety factors, (3) the occurrence of extreme environmental events such as hurricanes and earthquakes, (4) the non-replacement, repair or bypass of the sockets where large cable slips were observed, and (5) the addition of auxiliary cables as isolated cables.

More studies are required to characterize the relationship between cable safety factor, geometry of wire splay, and zinc properties to determine the service life of cable-socket assemblies. In the meantime, the risk of socket failure can be mitigated by controlling the factors that contributed to the failure of the telescope's sockets: (1) controlling the number and geometry of splayed-out wires during cable socketing, (2 and 3) designing cable systems with larger safety factors under gravity and transient loads,

(4) monitoring the cable slip and slip rate after cable installation, and (5) designing cable systems with multiple adjacent cables on each span.

Our analysis indicates that the excessive cable slips and eventual cable failures would not have occurred if the cable system had been designed with a safety factor of at least 3.0 under gravity loads, and we recommend using a safety factor of at least 4.0 under transient loads. When monitoring cable sockets after installation, limiting the allowable cable slip to one-sixth of the cable diameter as recommended by AASHTO[3] is a reasonable criterion and would have triggered the bypass or replacement of the first socket that failed.

[3] American Association of State Highway and Transportation Officials (AASHTO). AASHTO M 277-06. Standard Specification for Wire Rope and Sockets for Movable Bridges. 2019.

Table of Contents

List of Appendices

1.0 Introduction

The Arecibo Telescope (the telescope) was a radio telescope located at the Arecibo Observatory (AO) in Arecibo, Puerto Rico. The telescope collapsed on December 1, 2020, after 57 years of service. The collapse occurred after two structural cables failed in August and November 2020. In February 2021, we were retained by the University of Central Florida, who operates the Observatory on behalf of the National Science Foundation through a cooperative agreement, to investigate the causes of the cable failures and telescope collapse.

Our investigation encompasses the review of relevant documents, such as design drawings, historical and monitoring data, and field observations made over the life of the structure and during its progressive failure in 2020. We also reviewed the reports on the first cable failure by Wiss, Janney, Elstner Associates (WJE)[4] and the NASA Engineering and Safety Center (NESC).[5] The WJE report includes the NESC report, and therefore our references to the WJE report also refer to the NESC report. As a second focus of the investigation, we recovered failed and intact elements from the collapsed structure and performed a set of laboratory studies and tests. Finally, we performed a set of analyses using computer models of the full telescope structure and some of its components.

The two cable failures that occurred before the collapse and the third cable failure that triggered the collapse all happened near or within zinc-filled spelter sockets at cable ends. No cable failed away from a socket prior to collapse. Each failure involved both the rupture of some of the cable's wires and a deformation of the socket's zinc, and is therefore the failure of a cable-socket assembly. While the terms *cable failure* and *socket failure* are used in this report for the sake of concision, they always refer to the failure of a cable-socket assembly.

This report is organized into three main sections: Background (section 2.0), Observations (section 3.0), and Analysis (section 4.0). The Background section describes the telescope and cable system, and summarizes the structure's history including construction, maintenance, environmental and operational loads, and cable failures leading up to the collapse. The Observations section presents the evidence relevant to cable and socket condition and behavior observed in the field before and after the first cable failure, and in the laboratory after the collapse. The results of two sets of analyses are presented in the Analysis section: a global analysis of the telescope structure to determine the forces experienced by the cables and sockets over time, and a local analysis of zinc-filled spelter sockets to identify the factors that contributed to the failure of some of the telescope's sockets. Lastly, the report provides a brief discussion (section 5.0) of the above information and findings, as well as recommendations (section 6.0) for future work.

This report is intended to provide a brief overview of the investigation and concisely describe the results of many hours of work. More detailed descriptions and explanations of the steps and processes are provided in the attached appendices. In addition to this report, WJE and NESC provided an excellent report on the first socket failure. Much of the work was being performed in parallel, but independently from each other to a large extent.

---

[4] Wiss, Janney, Elstner Associates (WJE). *Auxiliary Main Cable Socket Failure Investigation.* June 21, 2021. Draft report provided by WJE.

[5] NASA Engineering and Safety Center (NESC). *Arecibo Observatory Auxiliary M4N Socket termination Failure Investigation.* NASA/TM-20210017934. NESC-RP-20-01585. June 2021.

2.0 Background

2.1 Telescope Overview and History

The Arecibo Telescope was the largest single-aperture radio telescope in the world when it was constructed in 1963, and remained so until 2016. The primary reflector of the telescope was a fixed spherical dish suspended just above the ground and 1,000 feet in diameter (Figure 1). The radio feeds of the telescope were located 500 feet above the primary reflector on a suspended structure (Figure 2) that was connected to three concrete towers with steel cables. The suspended structure had several moveable parts, which allowed one to position the radio feeds and conduct other experiments. AO is owned by the US National Science Foundation (NSF) and was managed by Cornell University from its opening to 2011. Management was transferred to a consortium led by SRI International in 2011, and to another consortium led by the University of Central Florida in 2018.

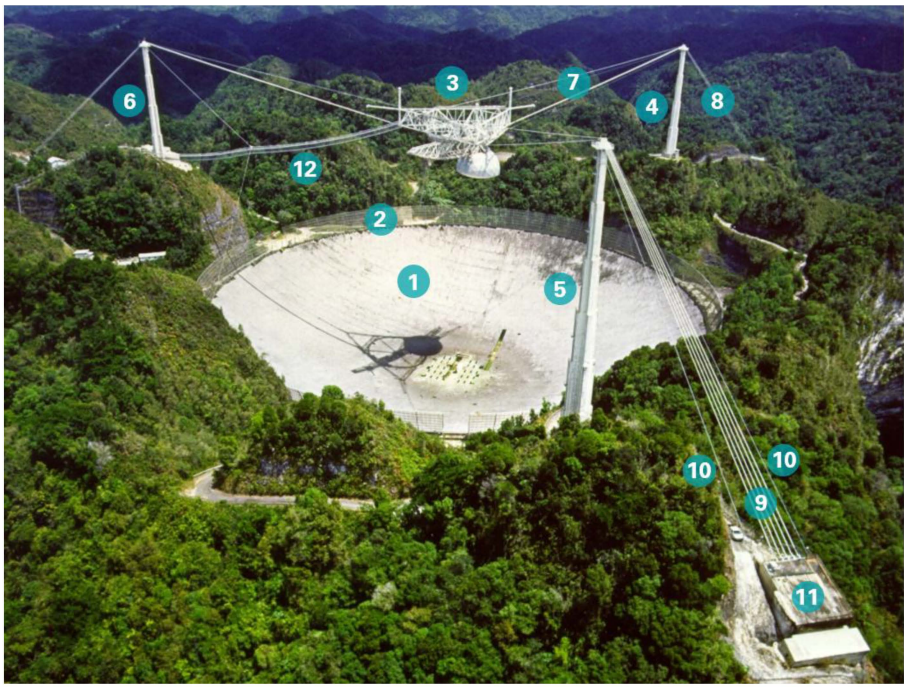

1 Primary reflector
2 Ground screen
3 Suspended structure
4 Tower 4
5 Tower 8
6 Tower 12
7 Tower 4 mains
8 Tower 4 backstays
9 Tower 8 original backstays
10 Tower 8 auxiliary backstays
11 Backstay anchorage
12 Waveguide

Figure 1: Overview of telescope structure after second upgrade *(photo: NSF).*

The original telescope was completed in 1963. The suspended structure was supported with 12 main cables (original mains) – four running in parallel from each tower top. The towers were tied to the ground with 15 backstay cables (original backstays) – five running in parallel from each tower top. The suspended structure was also tied directly to the ground with six inclined tiedowns. These tiedowns were modified in 1974 during a first upgrade of the telescope (Figure 3), with no significant change to the tension in the other cables.

During the second upgrade of the telescope (Figure 3) completed in 1997, the weight of the suspended structure was increased by 40 percent with the addition of the Gregorian and other structural changes. To support the weight increase, six additional main cables (auxiliary mains) and six additional backstay cables (auxiliary backstays) were added to the cable system. Each auxiliary main and backstay was an isolated cable and did not run in parallel with other cables. The inclined tiedowns were replaced with vertical tiedowns equipped with linear actuators (jacks) to minimize the elevation fluctuation of the

suspended structure during day-night temperature cycles. The structure was not significantly modified after the second upgrade. Additional information on the structure's history is provided in Appendix C.

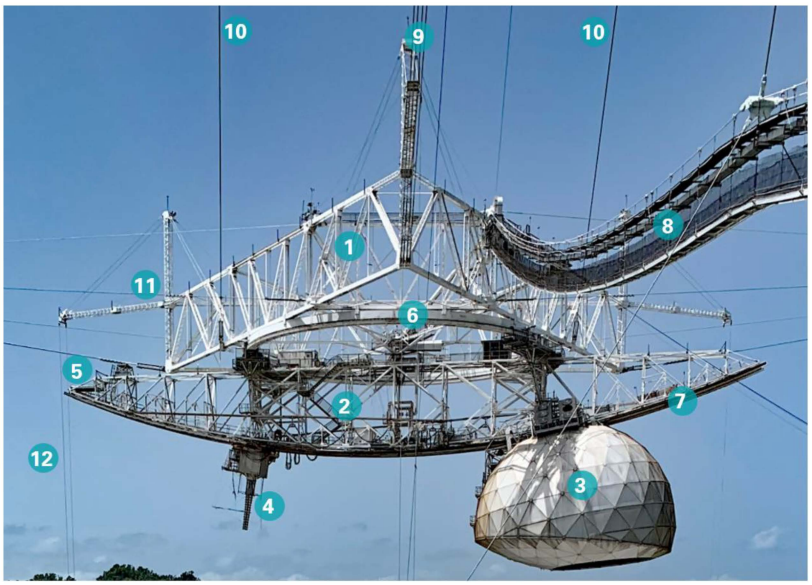

1 Platform
2 Azimuth arm
3 Gregorian
4 Line feed
5 Counterwight
6 Ring girder
7 Azimuth tracks
8 Waveguide
9 Original mains
10 Auxiliary mains
11 Outrigger
12 Tiedowns

Figure 2: Main components of telescope suspended structure after second upgrade
(photo: Mario Roberto Duran Ortiz, Wikipedia - CC BY-SA 4 0).

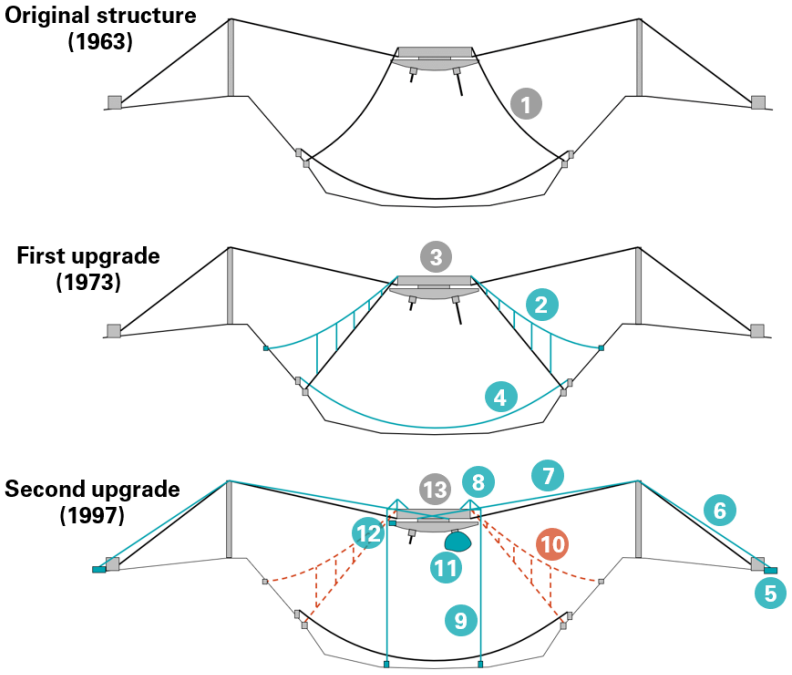

1 Inclined tiedowns sagging under self-weight
2 New carrier cables and hangers removing sag from tiedowns
3 New equipment on suspended structure
4 New primary reflector surface
5 New anchorages for auxiliary backstays
6 New auxiliary backstays
7 New auxiliary mains
8 New tiedown outriggers
9 New vertical tiedowns
10 Removed inclined tiedowns
11 New Gregorian replacing second carriage house
12 New counterweight
13 New equipment and reinforcement on suspended structure

Figure 3: Major structural upgrades of the telescope.

2.2 Cable System Design and Construction

The *cable system* of the telescope consisted of the main and backstay cables supporting the suspended structure above the reflector, and the cable-socket assemblies at the cable ends. The cables were anchored into the sockets, which in turn were connected to the platform, towers, and backstay anchorages. The loads acting on the telescope structure (gravity, wind, earthquakes, etc.) induced stresses in the cables, and the resultant of the stresses over a cable's section is referred to as the cable's *tension* in this report.

2.2.1 Cables and Sockets

After the second upgrade, the telescope structure included more than four miles of steel cables. Each cable was a single strand made of 126 to 216 galvanized steel wires arranged in concentric layers (Figure 4). The wires were woven helicoidally, and the pitch of the helix alternated between layers. The cable diameter, number of wires and wire diameter varied between cable types (Table 1).

1 Core 2 Inner layer wire
3 Outer layer wire

Figure 4: Side and section views of an auxiliary backstay cable.

1 Steel cable 2 Zinc casting
3 Steel socket 4 Socket shoulder

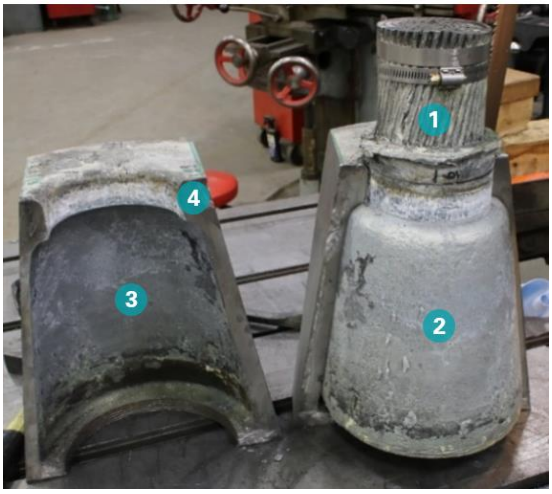

Figure 5: Zinc casting of auxiliary backstay socket B4N_G *(photo: Socotec).*

Table 1: Main and backstay cable properties

	Original Mains	Original Backstays	Auxiliary Mains	Auxiliary Backstays
Cable Diameter	3"	3 1/4"	3 1/4"	3 5/8"
Number of Wires	168	216	126	142 (+23)
Wire Diameter	13/64"	13/64"	1/4"	1/4" (3/16")
Minimum Breaking Strength[A]	1,044 kip	1,212 kip	1,314 kip	1,614 kip
Number of Cables	12	15	6	6

[A] 1 kip = 1,000 pounds

A key property of each cable type is its *Minimum Breaking Strength* (Table 1). Structural cables are fabricated to meet the requirements of a standard, such as ASTM A586[6] for the telescope's auxiliary cables. A standard provides several manufacturing specifications, one of which is a Minimum Breaking Strength. A brand new cable is not expected to fail under any tension lower than its Minimum Breaking Strength. The actual breaking strength of a cable is in fact expected to be somewhat higher than the Minimum Breaking Strength when the cable is new, but it may be lower when the cable is damaged or corroded. The Minimum Breaking Strength is therefore a reference value used to design cable systems, but it is not predictive of the actual breaking strength of a particular cable after a given time in service.

The cables of the telescope were terminated with zinc-filled spelter sockets at both ends (Figure 5, Figure 6). A spelter socket is a steel block with a cone-shaped cavity where the cable is inserted (Figure 6-1) and the cable's wires are spread, splayed or broomed out (Figure 6-2) before the cavity is filled with molten zinc (Figure 6-3). The zinc bonds to the wires and becomes a solid conical block after solidifying, which prevents the cable from exiting the socket, thereby anchoring the cable in the socket. The cable-socket assembly is typically pre-stretched prior to installation, causing the zinc block to seat into the socket and resulting in a little extrusion of the zinc, which is referred to as cable slip (Figure 6-5). Spelter sockets can be connected to supporting structures in a variety of ways, and three types of socket-to-structure connections were used in the telescope (Figure 7). Despite the exterior differences, the internal cable-to-socket connection was similar for all of the telescope's sockets. Most of the telescope's sockets, including socket B4N_G shown in Figure 5, featured a shoulder that breaks the cone's slope near the front of the socket.

Cable manufacturers typically verify through testing that the cable-socket assembly is stronger than the connected cable. In other words, the cable-socket assembly is not expected to fail before the cable. Samples of the auxiliary main and backstay cables were tested in 1993 before the second upgrade of the telescope. For both samples, the first wire ruptures occurred several feet away from the sockets and under a load higher than the cable's Minimum Breaking Strength.

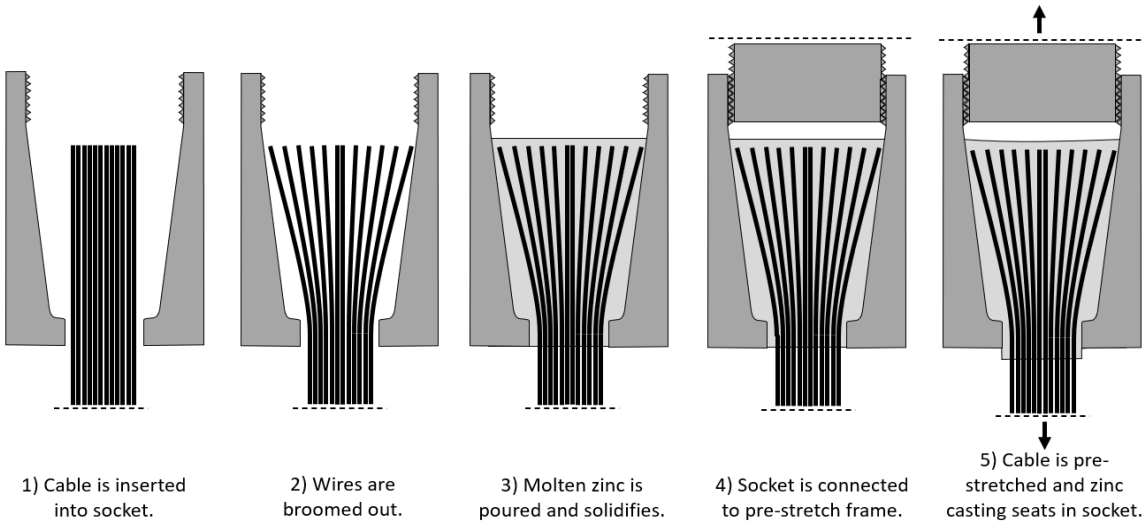

Figure 6: Cable socketing and pre-stretching process.

[6] American Society for Testing and Materials (ASTM). *ASTM A586-18. Standard Specification for Metallic-Coated Parallel and Helical Steel Wire Structural Strand.* 2018.

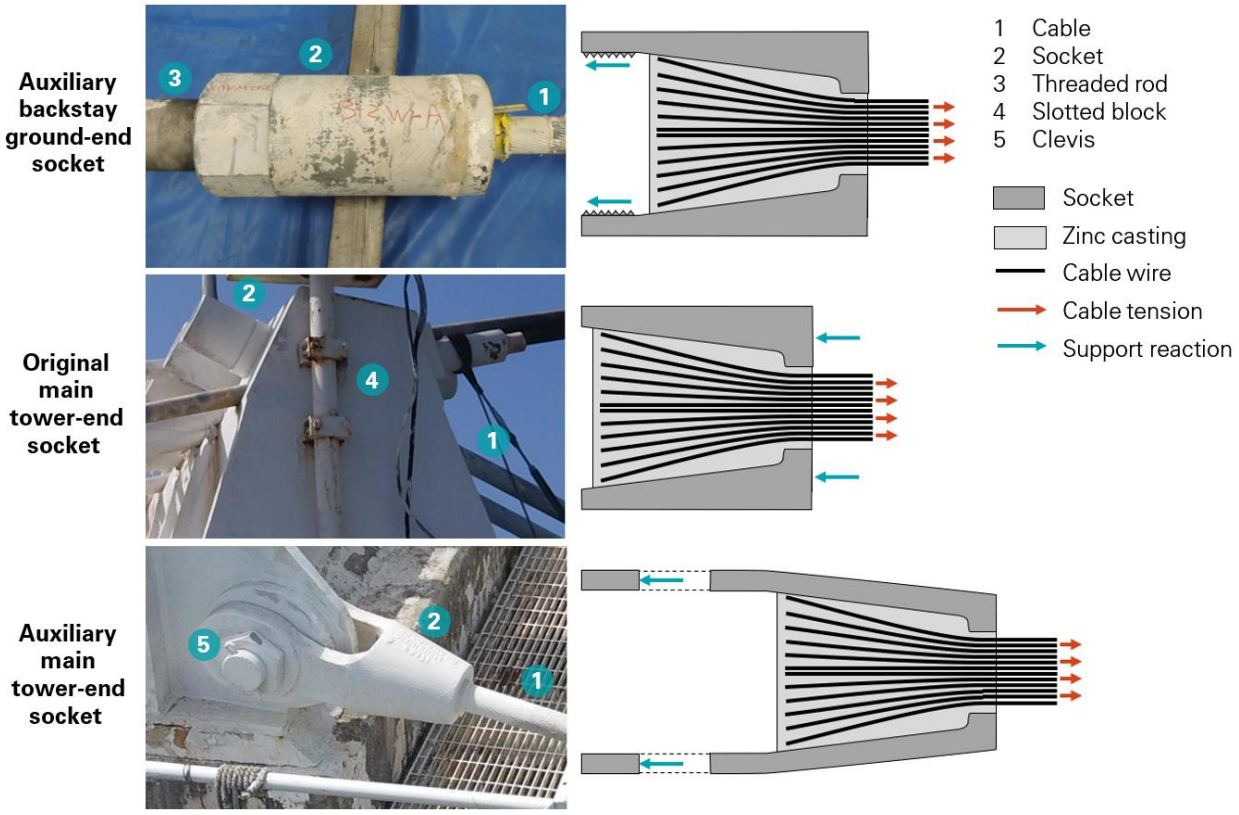

Figure 7: Three zinc-filled spelter socket designs used in the telescope
(top photo: Socotec; middle and bottom photos: NAIC Arecibo Observatory, a facility of the NSF).

2.2.2 Safety Factors

When selecting a cable type and proportioning a cable's diameter, the designer uses a *safety factor* to ensure that the actual breaking strength of the cable is beyond the expected cable tension and reduce the risk of failure to an acceptably low probability. Throughout this report, the safety factor is notional and defined as the cable's Minimum Breaking Strength divided by the cable's actual tension. For a given cable, this safety factor only varies with the cable's tension: if the tension increases due to environmental or situational conditions, the safety factor decreases. While the true safety factor also decreases when a cable is damaged, it is not used in this report as the condition of each cable in-place is not precisely known.

Several structural design standards prescribe a minimum safety factor to be used when designing cable systems, and the prescribed safety factor varies between standards. Standards commonly used nowadays include ASCE-19,[7] which prescribes a safety factor of 2.2 for cables used in building structures, and AASHTO LRFD-8,[8] which prescribes a safety factor of up to 4 for bridge cables. A

[7] American Society of Civil Engineers (ASCE). *ASCE 19-16. Structural Applications of Steel Cables for Buildings*. 2016.

[8] American Association of State Highway and Transportation Officials (AASHTO). *AASHTO LRFD-8. Bridge Design Specifications*. 8th edition. 2017.

precursor of ASCE-19 was AISI,[9] which was first released shortly after the telescope's original construction and prescribed a safety factor of 2.5.

The drawings for the original (1963) and the upgraded (1997) telescope structure specify the Minimum Breaking Strength and expected cable tensions (Figure 8). The average safety factor in the original cable system is approximately 2 under the self-weight of the telescope, and 1.67 considering a 140-mph wind speed in addition to self-weight (Table 2). The second upgrade of the telescope (1997) considered a reduced wind speed of 110 mph for the cable system design, and required the tiedowns be partially released before the occurrence of major windstorms to reduce the cable tensions. As a result, the second upgrade of the telescope increased the average safety factor to 2.25 under self-weight, and 2.15 during the design windstorm (Table 2). As a point of reference, we define the term *design tensions* as those in Table 2, which were extracted from the design documents shown in Figure 8.

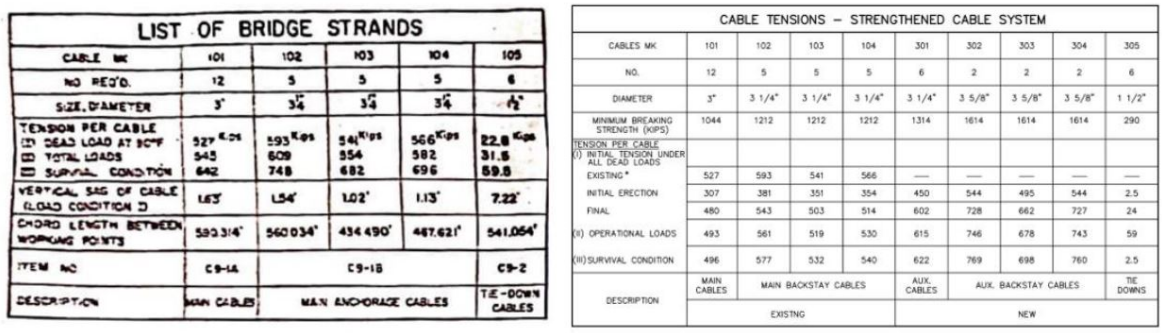

LIST OF BRIDGE STRANDS

CABLE MK	101	102	103	104	105
NO REQ'D.	12	5	5	5	6
SIZE, DIAMETER	3"	3 1/4"	3 1/4"	3 1/4"	1 1/2"
TENSION PER CABLE (I) DEAD LOAD AT 90°F	527 Kips	593 Kips	541 Kips	566 Kips	22.8 Kips
(II) TOTAL LOADS	545	609	554	582	31.5
(III) SURVIVAL CONDITION	642	748	682	696	59.5
VERTICAL SAG OF CABLE (LOAD CONDITION I)	1.63'	1.54'	1.02'	1.13'	7.22'
CHORD LENGTH BETWEEN WORKING POINTS	593.314'	560.034'	434.490'	487.621'	541.054'
ITEM NO	C9-1A	C9-1B			C9-2
DESCRIPTION	MAIN CABLES	MAIN ANCHORAGE CABLES			TIE-DOWN CABLES

CABLE TENSIONS – STRENGTHENED CABLE SYSTEM

CABLES MK	101	102	103	104	301	302	303	304	305
NO.	12	5	5	5	6	2	2	2	6
DIAMETER	3"	3 1/4"	3 1/4"	3 1/4"	3 1/4"	3 5/8"	3 5/8"	3 5/8"	1 1/2"
MINIMUM BREAKING STRENGTH (KIPS)	1044	1212	1212	1212	1314	1614	1614	1614	290
TENSION PER CABLE (I) INITIAL TENSION UNDER ALL DEAD LOADS									
EXISTING*	527	593	541	566	—	—	—	—	—
INITIAL ERECTION	307	381	351	354	450	544	495	544	2.5
FINAL	480	543	503	514	602	728	662	727	24
(II) OPERATIONAL LOADS	493	561	519	530	615	746	678	743	59
(III) SURVIVAL CONDITION	496	577	532	540	622	769	698	760	2.5
DESCRIPTION	MAIN CABLES	MAIN BACKSTAY CABLES			AUX. CABLES	AUX. BACKSTAY CABLES			TIE DOWNS
	EXISTING				NEW				

Figure 8: Cable tension tables provided in original (left) and second upgrade (right) structural drawings
(images: structural drawings, courtesy of NAIC Arecibo Observatory, a facility of the NSF).

Table 2: Cable design tensions and safety factors

		Minimum Breaking Strength [kip]	Design Tension in Original Structure [kip (SF)][D]		Design Tension after Second Upgrade [kip (SF)][D]	
			Self-Weight Only	Self-Weight + Max. Wind Load	Self-Weight Only	Self-Weight + Max. Wind Load
Original Cables[B]	**Mains**	1,044	527 (1.98)	642 (1.63)	480 (2.18)	496 (2.10)
	T4 Backstays	1,212	593 (2.04)	748 (1.62)	543 (2.23)	577 (2.10)
	T8 Backstays	1,212	541 (2.24)	682 (1.78)	503 (2.41)	532 (2.28)
	T12 Backstays	1,212	566 (2.14)	696 (1.74)	514 (2.36)	540 (2.24)
	Average[A]		(2.07)	(1.67)	(2.26)	(2.16)
Auxiliary Cables[C]	**Mains**	1,314	-	-	602 (2.18)	622 (2.11)
	T4 Backstays	1,614	-	-	728 (2.22)	769 (2.10)
	T8 Backstays	1,614	-	-	662 (2.44)	698 (2.31)
	T12 Backstays	1,614	-	-	727 (2.22)	760 (2.12)
	Average[A]	-	-	-	(2.24)	(2.15)

[A] Average weighted by number of cables.
[B] Minimum Breaking Strengths reported are based on ASTM A586.
[C] Minimum Breaking Strengths reported are as indicated in drawings for second upgrade.
[D] 1 kip = 1,000 pounds, SF = safety factor.

[9] American Iron and Steel Institute (AISI). *Tentative Criteria for Structural Applications of Steel Cables for Buildings.* 1966.

2.2.3 Installation and Tensioning

The original cables of the telescope were laid out as groups of parallel cables: groups of four cables for the mains, and groups of five cables for the backstays. The cables in one group are spaced approximately one foot apart and share the load from tower or platform equally. This is confirmed by noting equal sag in the cables.

We were unable to find any detailed record of the cable tensioning operations during the original construction and the second upgrade, but the general methods are known. During construction, the platform was lifted in place with temporary cables before installing and tensioning the permanent cables. During the second upgrade, the new auxiliary cables were tensioned gradually as load was added to the suspended structure. It is therefore unlikely that the permanent cables experienced tensions significantly higher than the design tensions (Table 2) during construction. Surveys performed between 1972 and 2016 confirm that under self-weight, the actual cable tensions were consistent with the design tensions. Additional details on the construction and upgrade sequences are provided in Appendix C.

2.3 Cable System Maintenance

Throughout the life of the telescope, the condition of the cable system and the maintenance operations were recorded locally by the AO staff. Occasional structural inspections were also performed by the Engineer of Record Amman & Whitney (AW) between 1972 and 2011. The available information is generally less comprehensive and detailed after the second upgrade in 1997, and the scope of the inspections performed by AW was reduced. Details of the cable system's condition and maintenance history are provided in Appendix D.

Paint Condition

The cables were painted to prevent corrosion, and the paint was well-maintained before the second upgrade in 1997. After the upgrade, AW reported in 2003 and 2011 that the paint on the original cables was in poor condition, with corrosion of the steel wires at some locations. No record of a comprehensive re-painting of the original cables was found after the second upgrade.

Moisture Exclusion System

In the late 1960s, AO observed that the cables were not fully airtight in the transition zone between cable and socket, and determined that this could lead to corrosion within the cable due to moist air intrusion and condensation. In 1972, a system of sleeves, air compressors and dryers was installed at the lower end of the cables to circulate dry air through the cables and prevent accumulation of moisture (Figure 9). The same moisture exclusion system was installed on the auxiliary cables during the second upgrade in 1997. While the system appeared to be functional, condensation was occasionally reported in some of the dry air sleeves between 2002 and 2011. We also observed water accumulation in some of the dry air sleeves during our site visits before and after the collapse.

Vibrations

The cables of the telescope experienced wind-induced vibrations immediately after construction in 1964. Stockbridge dampers (Figure 10) were installed to mitigate the vibrations and appear to have been effective, even though vibrations continued to be reported between 1970 and 2011. The vibrations were

reported as "slight to moderate"[10] and seem to have occurred relatively infrequently and only under specific wind conditions.

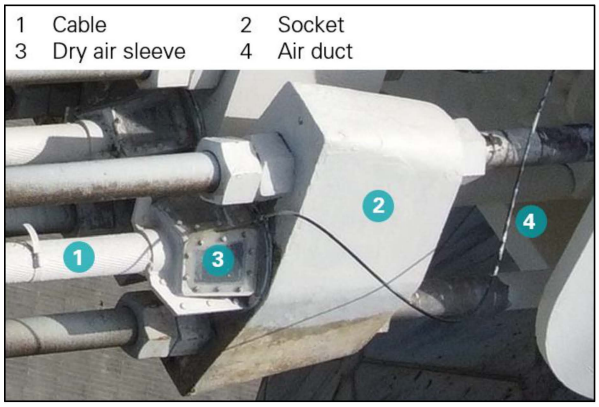

Figure 9: Dry air sleeve on M8-1_P socket
(photo: NAIC Arecibo Observatory, a facility of the NSF).

Figure 10: Stockbridge dampers on original M4 cables
(photo: NAIC Arecibo Observatory, a facility of the NSF).

Repairs and Modifications

Apart from the second upgrade, three significant changes were made to the cable system. In 1981, one of the original backstays of Tower 12 was replaced after six wire breaks were discovered in the cable over time. Then in 1997, a threaded rod connecting the platform-end socket of cable M8-4 was accidentally damaged while implementing the second upgrade of the telescope. A structural bypass was installed to catch the socket should the damaged rod fail (Figure 11). In 2014, a splice near the tower end of the same M8-4 cable was bypassed after multiple wire breaks were discovered during an inspection (Figure 12).

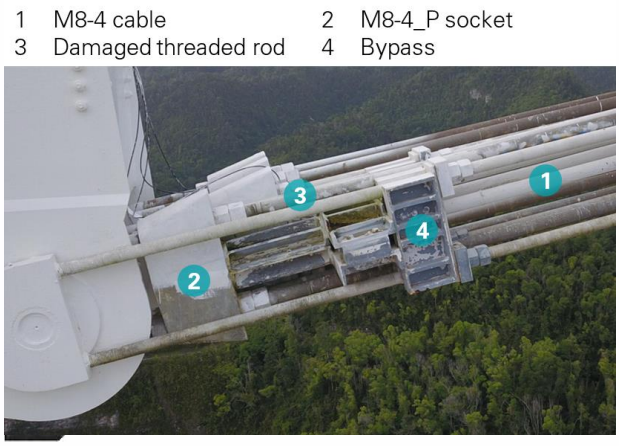

Figure 11: Damaged rod bypass at platform end of cable M8-4
(photo: NAIC Arecibo Observatory, a facility of the NSF).

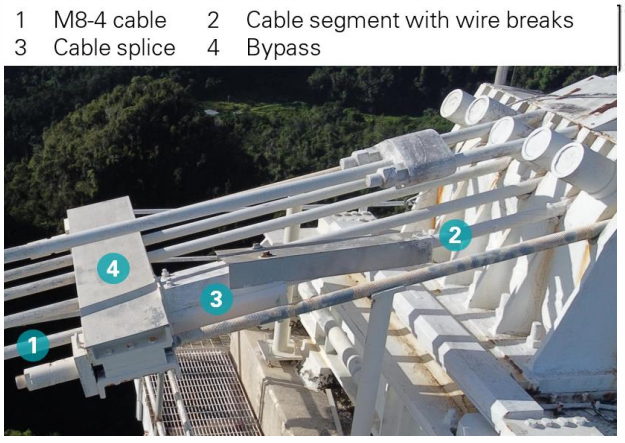

Figure 12: Cable splice bypass near tower end of cable M8-4
(photo: NAIC Arecibo Observatory, a facility of the NSF).

[10] Ammann & Whitney. *Arecibo Radio Telescope Structural Condition Survey*. 2011. Report retrieved from Cornell University archives.

2.4 Load Effects on Cable System

2.4.1 Typical Conditions

In normal operating conditions, the telescope structure was subjected to significant load effects from three sources: its own weight, the movement of the azimuth arm, line feed and Gregorian during operation, and the day-night temperature cycles.

Suspended Structure Weight

The weight of the suspended structure increased significantly during the second upgrade in 1997, but it also varied before and after the upgrade as modifications were made to the structure and its equipment (Table 3). Details on the suspended structure's weight are provided in Appendix C.

Table 3: Suspended structure weight

Year	Structure Configuration	Source	Suspended Structure Weight
1963	Original	Original structural drawings	1,220 kip
1995	Original	Cable tensioning sequence for second upgrade	1,225 kip
1997	Upgraded	Cable sag survey after second upgrade	1,789 kip
2020	Upgraded	Cable sag survey after first cable failure	1,825 kip

Telescope Operation

The operation of the telescope changed the distribution of cable tensions. As shown in Figure 13, the suspended structure of the upgraded telescope consisted of a fixed platform supporting a moving azimuth arm, Gregorian and line feed. When the telescope was operating, the azimuth arm rotated about the center of the platform, while the Gregorian and line feed slid along the bottom of the azimuth arm. These displacements shifted the position of the structure's center of mass, which was balanced by changes in cable tensions. A sample of a weekly data log recording the positions of the azimuth arm, Gregorian and line feed is shown in Figure 14. The first half of the week is representative of the most common operating mode of the telescope, with the azimuth arm and Gregorian moving slowly and completing a few cycles per day. The second half of the week is representative of another operating mode of the telescope, where the Gregorian and line feed are fixed while the azimuth arm spins rapidly and continuously, with approximately four revolutions per hour. The Gregorian was installed during the second upgrade of the telescope to replace a carriage house, which was significantly lighter than the Gregorian. As a result, the operation of the telescope had a more significant impact on the cable forces in the upgraded structure than in the original structure.

Temperature Effects

The fluctuations in air temperature and solar radiation caused the materials of the telescope's structure to expand and contract, which affected the cable tensions. The ambient air temperature was recorded by a weather station located on the telescope's platform. The data indicates an average day-night temperature range of 12.3°F with no significant changes between seasons. In addition, after the first cable failure in 2020, six auxiliary cable sockets were instrumented by WJE with temperature sensors. We monitored the data and measured an average daily temperature range of 14.8°F on the steel surfaces. Details are provided in Appendix I.

The drop in temperature at night caused the telescope's cables to contract and the platform to rise as a result. The accuracy of the telescope's observations was affected by changes in platform elevation. To mitigate these fluctuations, the upgraded structure was equipped with an active tiedown system where electro-mechanical jacks pulled on the tiedowns at night to counter the rise and keep the platform at a constant elevation (Figure 15). A log of the tiedown forces since 2004 indicates that the total tiedown force increased by an average of 60 kip at night under the combined effect of temperature and jack pull-down, which increased the tensions in the entire cable system. The original structure was only equipped with passive tiedown cables, and therefore the impact of day-night cycles on the cable tensions was less significant.

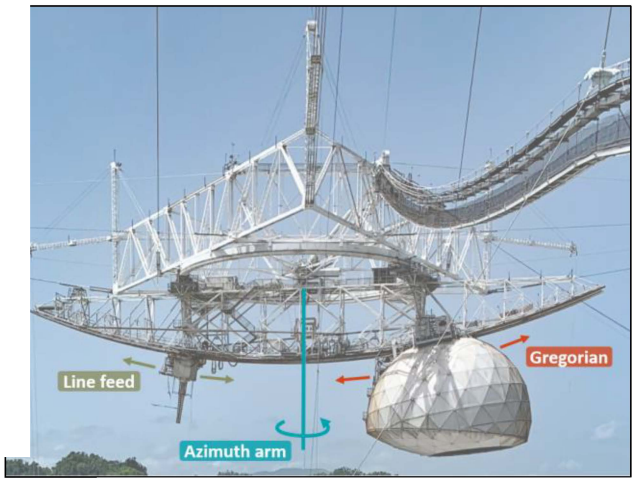

Figure 13: Moveable parts of suspended structure
(photo: Mario Roberto Duran Ortiz, Wikipedia - CC By-SA 4.0).

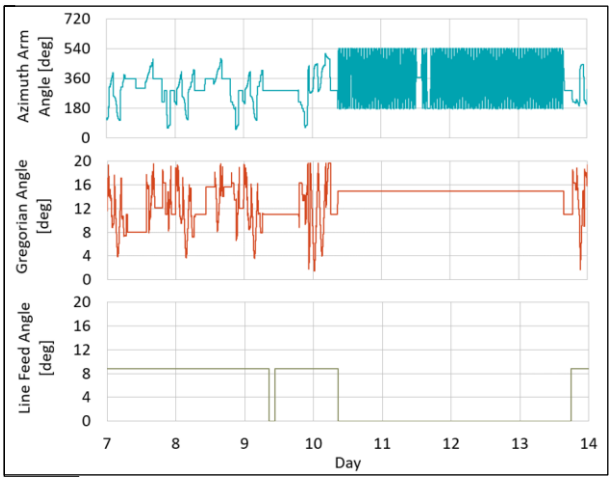

Figure 14: Positions of azimuth arm, Gregorian and line feed during one week of telescope operation (December 7, 2012 to December 14, 2012).

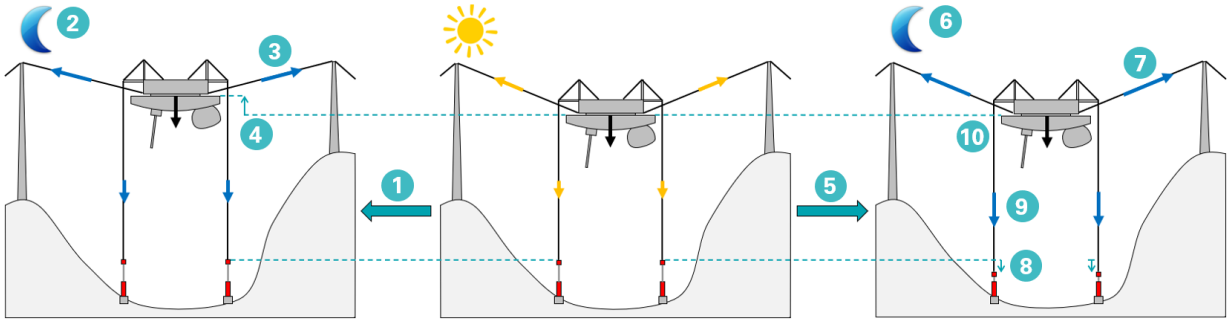

1 Day-night change without tiedown jacking
2 Air temperature drops by 12.3°F
3 Cable tensions increase
4 Platform rises

5 Day-night change with tiedown jacking
6 Air temperature drops by 12.3°F
7 Cable tensions increase
8 Tiedown jacks pull down
9 Total tiedown tension increases by 60 kip
10 Platform stays at same elevation

Figure 15: Tiedown jacks mitigating the impact of day-night temperature cycles on platform elevation in upgraded structure.

2.4.2 Extreme Environmental Events

The Island of Puerto Rico is often subjected to earthquakes and severe windstorms, including hurricanes. These extreme events induced transient loads on the telescope that affected the cable forces.

Windstorms

Tropical storms and hurricanes regularly impact Puerto Rico and introduced high sustained and fluctuating wind loads onto the telescope structure. Hurricane wind speeds were considered in the design of the telescope, with a design wind speed of 140 mph for the original structure and 110 mph for the first and second upgrades. The lower wind speed of 110 mph was determined by AW, the engineer for both upgrades, as corresponding to a 100-year return period. We did not find any document providing the basis for the original wind speed of 140 mph. A wind tunnel study was performed before the second upgrade, with the scope limited to determining the pressures on the Gregorian dome.

The instantaneous wind speed and direction were monitored continuously and logged every second by the weather station on the telescope's platform. In the data log from 2005 to 2020, the highest instantaneous wind speed was 108 mph and occurred during Hurricane Maria on September 20, 2017 (Figure 16). AO did not experience the highest reported wind speed of the hurricane due to its inland location and mountainous terrain. The tiedown forces were also recorded continuously, and the data indicates that the suspended structure responded dynamically during strong wind events.

Earthquakes

Puerto Rico experiences frequent earthquakes due to its location between the North American and Caribbean tectonic plates. AO is equipped with a seismic monitoring station located on a hill of similar topography and geology as the hills where the telescope's towers and cable anchorages are built. The ground accelerations recorded at the station were therefore also experienced by the towers and anchors. Since the telescope's completion in 1963, more than 200 earthquakes of moment magnitude greater than 4.5 occurred within 200 km (125 miles) of AO, including a significant event of moment magnitude 6.4 on January 7, 2020 recorded by the station (Figure 17).

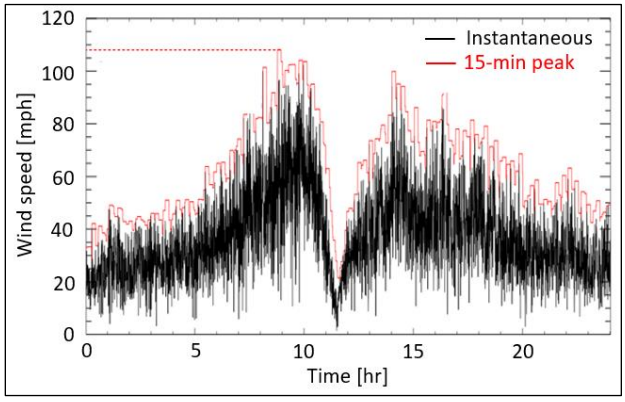

Figure 16: Wind speed recorded on telescope platform during Hurricane Maria on September 20, 2017.

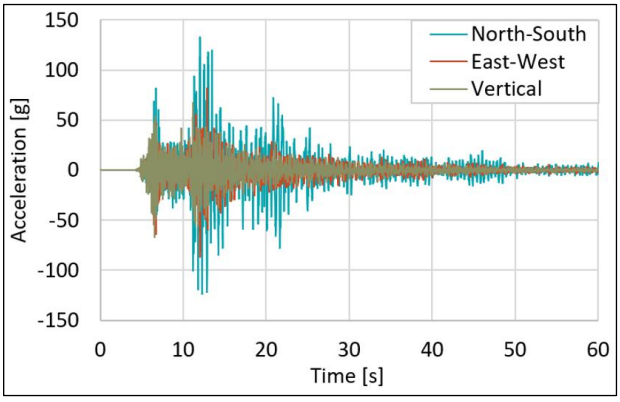

Figure 17: Ground accelerations recorded at AO during M6.4 earthquake on January 7, 2020.

2.5 Cable Failures and Collapse Sequence

At 2:36 AM local time on August 10, 2020, cable M4N pulled out of its socket at the top of Tower 4 (Figure 18). This first failure occurred as the telescope was operating normally, with the azimuth arm rotating with respect to the platform and the Gregorian shifting along the bottom of the azimuth arm. There were no particularly strong winds or any significant earthquake during that night. The telescope continued to operate (azimuth arm and Gregorian movement) for approximately 20 minutes after the cable failure, before being stopped by the operator. Several wire breaks were observed three days later in adjacent cables at the top of Tower 4, and likely occurred when M4N failed (details in Section 3.2.1).

On August 11, 2020, the AO staff placed the telescope in the stowed position. This operation involves moving the azimuth arm and Gregorian into predefined positions and locking them with pins, as was typically done before the arrival of significant windstorms. To reduce the forces in the remaining support cables, the jacks at the base of the tiedowns were fully extended. The azimuth arm, Gregorian and tiedown jacks were not moved again after August 11, 2020.

At approximately 10 PM local time on November 6, 2020, cable M4-4 failed at its socket at the top of Tower 4. This occurred in the absence of high winds and seismic activity. This second cable failure caused new wire breaks at the top of tower 4 (details in Section 3.2.1). In the three weeks following the second cable failure, multiple additional wire breaks occurred in the remaining main cables at the top of Tower 4 (details in Section 3.2.1).

At 7:54 AM local time on December 1, 2020, cable M4-2 failed at its socket at the top of Tower 4, once again without any significant wind or seismic activity. This third cable failure was immediately followed by the failure of the remaining two original mains at the top of Tower 4, initiating the fall of the suspended structure. The suspended structure swung down while still connected to Tower 8 and Tower 12, and impacted a cliff face between these two towers. During the fall, the azimuth arm detached from the platform and fell through the reflector. Finally, the top of the three towers broke off and fell (Figure 19).

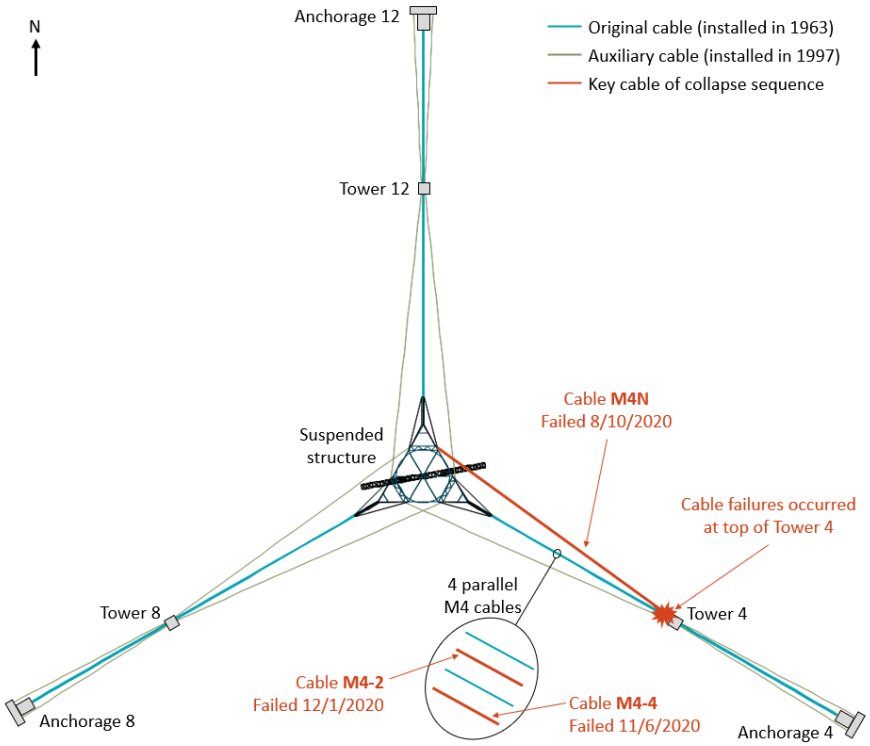

Figure 18: Cable failure locations.

Figure 19: Telescope collapse sequence, looking south.
(Still images of collapse video by NAIC Arecibo Observatory, a facility of the NSF. Intermediate still images are in provided Appendix E.)

3.0 Observations

While the cable system was designed with safety factors greater than 2, the telescope collapsed after the failure of several cable-socket assemblies. The focus of our investigation is therefore to understand the causes and mechanisms of these assembly failures. The failure investigation is performed based on three data sets: the telescope's maintenance and inspection records, the observations made between the first cable failure and the collapse, and the results of laboratory tests performed after the collapse.

3.1 Field Observations Prior to First Cable Failure

The information retrieved from the maintenance and inspection documents relevant to the socket's behavior and failures is summarized in the following, and more details are provided in Appendix D.

3.1.1 Wire Breaks

Each main and backstay cable is made of 126 to 216 steel wires, and individual broken wires were occasionally discovered near the cable ends throughout the structure's life (Figure 20). A total of 40 wire breaks had been reported before 2020 (Figure 22). No more than three wire breaks were reported at each cable end, with two exceptions: six breaks at the bottom of a backstay cable, which was subsequently replaced, and 12 breaks near a cable splice (Figure 21), which was subsequently bypassed. Only the breaks that occurred in the outer layer of wires were visible and therefore counted.

Figure 20: Single wire break observed at ground end of cable B4-1 on 12/12/1996
(photo: NAIC Arecibo Observatory, a facility of the NSF).

Figure 21: Multiple wire breaks observed at splice near tower end of cable M8-4 on 1/14/2014
(photo: NAIC Arecibo Observatory, a facility of the NSF).

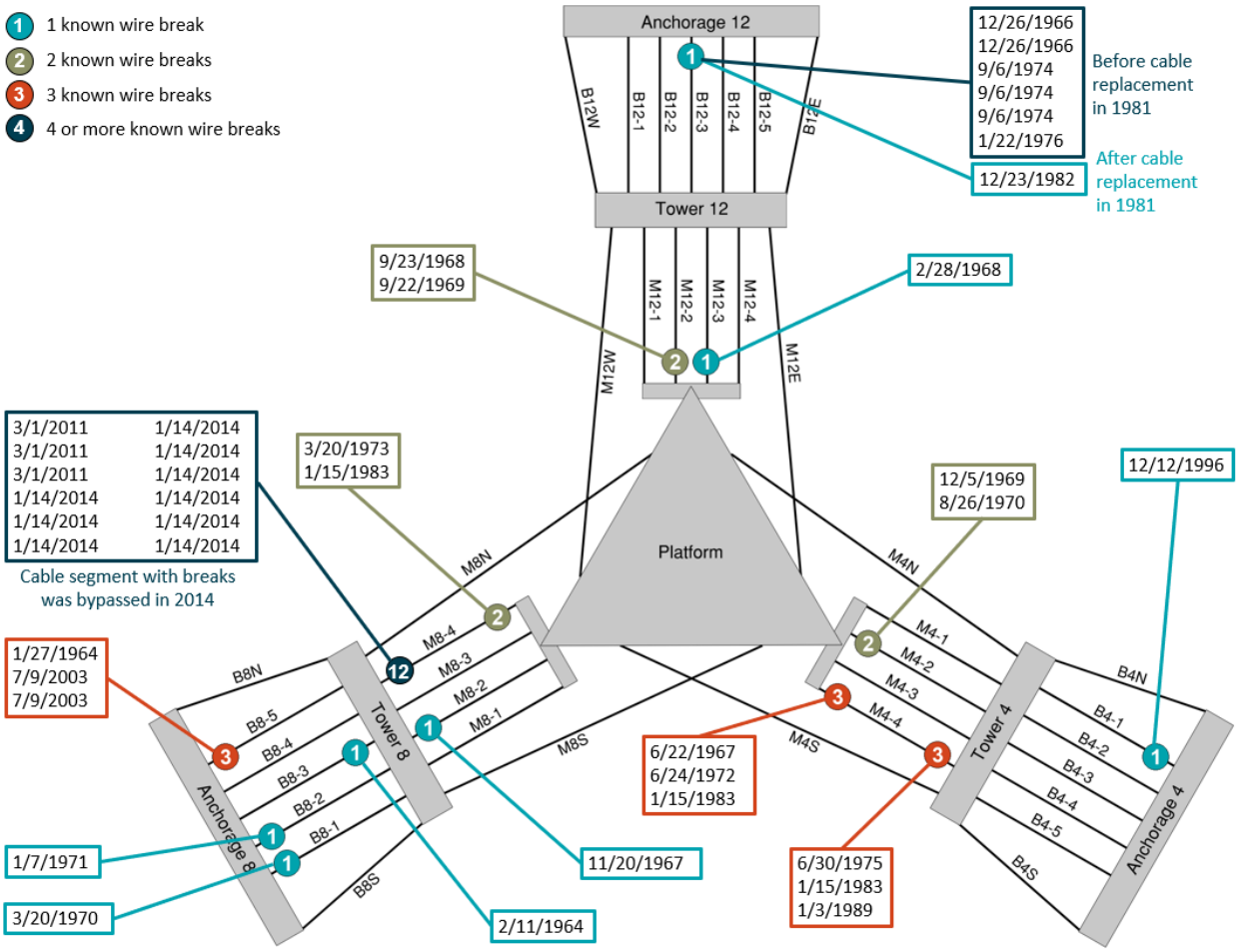

Figure 22: Wire break locations and report dates.

3.1.2 Cable Slips

It is not unusual for a cable to slightly displace out of a spelter socket when it is loaded as the zinc casting seats within the socket's cone. This cable slip is expected to remain relatively small and is exhibited by an extrusion of the zinc casting outside of the socket. For reference, one standard that addresses cable slip at spelter sockets is AASHTO M 277-06,[11] which limits the slip to one-sixth of the cable diameter when proof-loaded to 80 percent of the cable's Minimum Breaking Strength. For the telescope's main and backstay cables, this limit corresponds to a maximum slip between 0.5 and 0.6 inch.

Before failing on August 10, 2020, the end of cable M4N had slipped by more than one inch outside its socket at the top of Tower 4 (Figure 23). This slip is approximately one-third of the cable's diameter, and twice the AASHTO limit.

[11] American Association of State Highway and Transportation Officials (AASHTO). *AASHTO M 277-06. Standard Specification for Wire Rope and Sockets for Movable Bridges*. 2019.

Cable slips were observed but not consistently monitored and reported before August 2020. AW indicate in their inspection reports from 2003 and 2011 that they observed slips of up to 0.5 inch at the auxiliary cable sockets. It is not clear how many locations were inspected. Before the first cable failure, the AO staff observed significantly greater slips than reported by AW on at least two sockets: a 1.125-inch slip at the tower end of M4N (February 2019, Figure 23), and a 1.5-inch slip at the ground end of B12W (May 2018, Figure 24).

The cable slips were measured on all of the auxiliary cable sockets after the telescope's collapse, except for the first socket to fail (Figure 25). There is no consistent correlation between the cable slips and safety factors, which indicates that the cable slip at a socket does not only depend on the cable tension. The safety factors in Figure 25 are based on the actual cable tensions under gravity loads, determined through analysis (section 4.1.2).

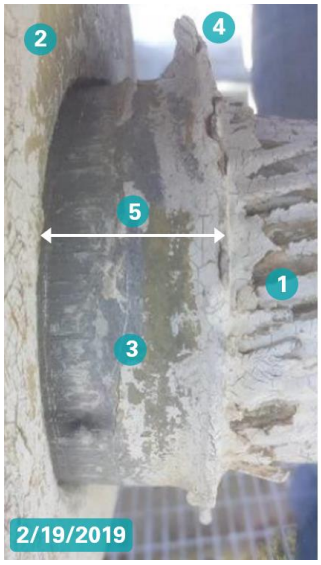

1 Cable
2 Socket
3 Zinc pulled out of socket
4 Zinc lip
5 Cable slip distance

Figure 23: Last known cable slip (1.125 inch) at socket M4N_T, where first cable failure occurred *(photo: NAIC Arecibo Observatory, a facility of the NSF).*

Figure 24: Cable slip increase measured at socket B12W_G *(photos: NAIC Arecibo Observatory, a facility of the NSF).*

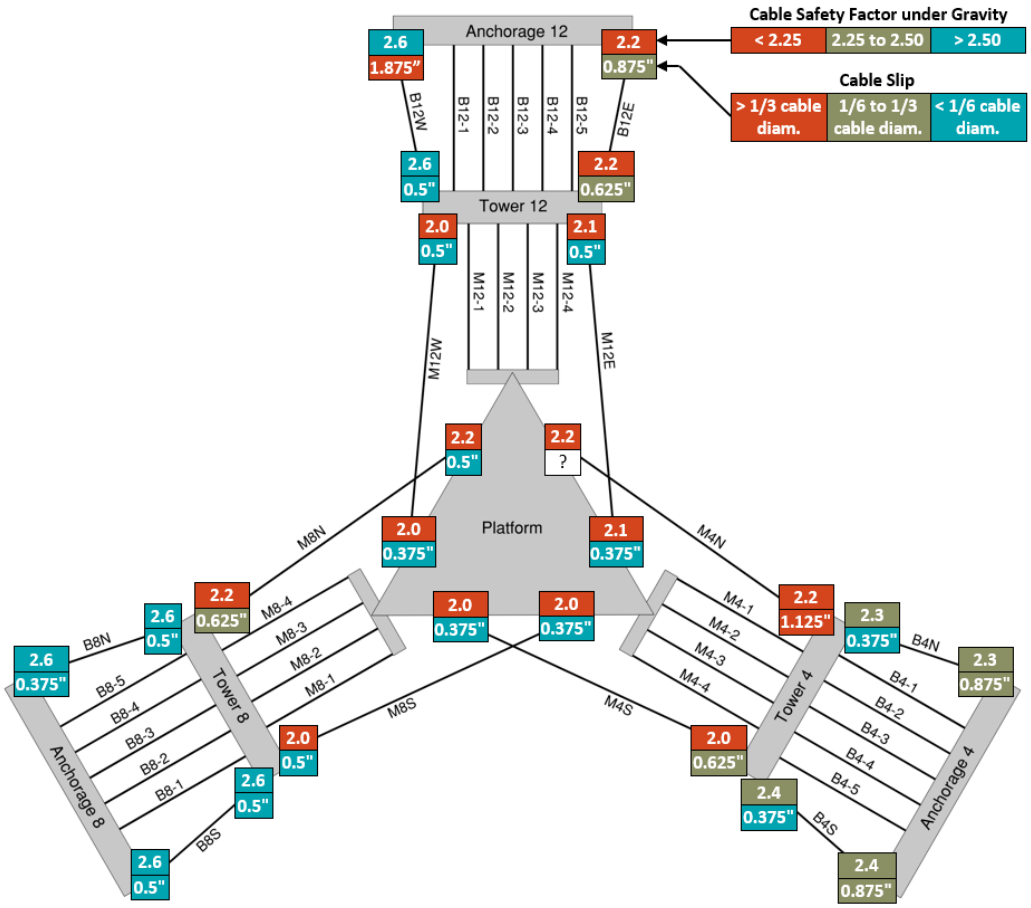

Figure 25: Cable safety factors and measured cable slips on auxiliary cable sockets.

3.2 Field Observations Between First Cable Failure and Collapse

After the first cable failure on August 10, 2020, the cable system was frequently inspected by AO until the collapse of the telescope on December 1, 2020. The inspections were visual and performed using drones to keep personnel at a safe distance from the damaged structure. While the cable ends at all three towers and three platform corners were regularly inspected, damage was only observed in the original main cables connecting to Tower 4 (M4 cables) and their sockets. Visible damage includes wire breaks, socket deformation, and full cable failures. The observed damage is summarized in this section, with additional details provided in Appendix E. The wire breaks counted in this section only include the breaks in the outer layer of wires, as breaks in the inner layers, if any, are not visible.

3.2.1 First Cable Failure

Based on the AO inspection records, the M4 cables had experienced eight wire breaks before the M4N failure (first cable failure): three breaks at each end of M4-4, and two breaks at the tower end of M4-2. The last of these wire breaks was reported in 1989.

The M4N failure caused four new wire breaks in M4-4 (Figure 26). Drone photos taken shortly after the failure show a significant deformation of the zinc casting of the M4-2 socket (Figure 26), although it is not known whether this deformation occurred before or during the M4N failure. The cracks and dip on the

casting's back surface indicate that a cylindrical casting core, whose diameter is approximately equal to the cable diameter, had moved within the socket.

In the three months between the M4N and M4-4 cable failures, the only visible changes are two new wire breaks, at the tower ends of M4-1 and M4-2.

The cable slips were measured at the tower and ground ends of the auxiliary cables after the first cable failure, and at the platform ends after the collapse (Figure 25). One-third of the cable slips exceeded the AASHTO limit of one-sixth of the cable diameter. The maximum cable slip was observed at the ground end of B12W, and had increased from 1.5 inches in May 2018 to over 1.75 inches in September 2020 (Figure 24).

1 Cable M4-1
2 Cable M4-2
3 Cable M4-3
4 Cable M4-4
5 Failed M4N_T socket
6 Chipped paint due to four wire breaks
7 Anchor block at top of Tower 4

8 Socket M4-1_T
9 Socket M4-2_T
10 Socket M4-3_T
11 Socket M4-4_T
12 Crack at back of M4-2_T zinc casting

Figure 26: Damage on original M4 cables at top of Tower 4 after first cable failure
(photos: NAIC Arecibo Observatory, a facility of the NSF).

3.2.2 Second Cable Failure

The failure of M4-4 on November 6, 2020 caused multiple new wire breaks in the remaining M4 cables: three breaks at the tower end of M4-1, a break at the tower end on M4-2, and four breaks at the platform end of M4-2. No change was observed on the other sockets. The breaks were documented shortly after the cable failure.

In the three weeks following the M4-4 failure, seven and five additional wires breaks were observed at the tower end of M4-1 and M4-2, respectively (Figure 27). The zinc casting of the M4-2 socket continued to deform with signs of crack movement at the back face of the casting (Figure 28).

1 Four wire breaks in M4-1
2 Two wire breaks in M4-2

3 11 wire breaks in M4-1
4 Seven wire breaks in M4-2

Figure 27: Wire break development after second cable failure
(photos: NAIC Arecibo Observatory, a facility of the NSF).

1 Failed end of M4-4 cable
2 Crack at back of M4-2_T zinc casting sealed before M4-4 failure

3 New crack at back of M4-2_T zinc casting due to further casting deformation

Figure 28: Evidence of socket casting core displacement after second cable failure
(photos: NAIC Arecibo Observatory, a facility of the NSF).

3.2.3 Third Cable Failure and Telescope Collapse

On December 1, 2020, the telescope collapsed immediately after the failure of cable M4-2 at the top of Tower 4, which was captured on a drone video (Figure 29). The video shows a wire break on M4-2, followed by the entire cable failure three seconds later and the failure of the remaining two M4 cables immediately after. After loss of support from Tower 4, the platform swung down away from Tower 4 and crashed into a cliff face between Tower 8 and Tower 12.

1 New wire break in M4-2 2 Complete failure of M4-2
3 Complete failure of M4-1 4 Complete failure of M4-3

Figure 29: Progressive failure of original main cables at top of Tower 4.
(still images of drone video by NAIC Arecibo Observatory, a facility of the NSF. Intermediate still images are provided in Appendix E.)

3.3 Post-Collapse Laboratory Study

Socket M4N_T, where the first cable failure occurred, was recovered on September 23, 2020 and sent to Kennedy Space Center for analysis by NESC in collaboration with WJE. The cable end that slipped out of M4N_T was recovered after the collapse in December 2020 and provided to NESC-WJE as well. The results of the M4N_T failure investigation are provided in WJE's report dated June 21, 2021.[12]

Additional sockets and cable samples were recovered from the site between December 2020 and July 2021. We worked with Socotec to perform a series of laboratory analyses and a full-scale load test. The laboratory observations are summarized in the following, and more details are provided in Appendix L through Appendix O.

3.3.1 Cable System General Condition

The original (1964) and auxiliary (1997) cables were in good general condition when the telescope collapsed. Several cable segments were taken apart to observe the condition of the inner layers of wires. As shown in Figure 30, moderate corrosion of the wires' galvanizing zinc and superficial corrosion of the wires' base steel was observed at some discrete locations. The remaining weight of galvanizing zinc was measured on wires taken from the outer layers of three original cables. After 57 years of service, more than 80 percent of the tested wires still had more galvanizing zinc than required for new Class A wires

[12] Wiss, Janney, Elstner Associates (WJE). *Auxiliary Main Cable Socket Failure Investigation*. June 21, 2021. Draft report provided by WJE.

per the standard applicable to the telescope's auxiliary cables.[13] Three fractured wires due to the development of stress-corrosion cracks were discovered in the inner layers of one cable sample.

Setting aside the cable slips and casting deformations, the original and auxiliary cable sockets were in good condition. Corrosion was observed on the zinc casting surfaces that were not in tight contact with the socket's steel, but this corrosion had no impact on the socket's strength.

Additional details on the cable and socket general conditions are provided in Appendices L and M.

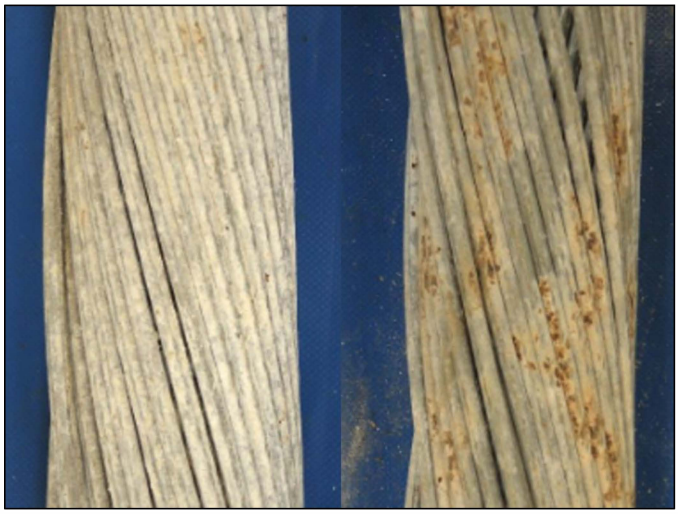

Figure 30: Oxidation of galvanizing zinc (left) and wire steel (right) in second wire layer of an original M4 cable *(photos: Socotec).*

Figure 31: Surface corrosion of B12W_G socket casting *(photo: Socotec).*

3.3.2 Wire and Zinc Properties

The auxiliary cables were specified by the design drawings to meet the ASTM A586 standard.[13] While no standard was specified for the original cables, they were required to have the same strength as prescribed in ASTM A586. Wire specimens taken from three original cables were tested to failure, and all specimens met the mechanical properties of ASTM A586 (160 ksi yield stress, 220 ksi ultimate stress, and four percent elongation in 10 inches). A 15-foot segment of auxiliary backstay cable was also load-tested, and the cable was able to carry a tension higher than the cable's Minimum Breaking Strength, which corresponds to the ultimate stress requirement of ASTM A586. The wire and cable tests are respectively detailed in Appendix L and Appendix N.

Zinc samples were taken from one original socket and three auxiliary sockets for chemical composition and tensile load testing. Three samples, including one from an original socket and two from auxiliary sockets, were evaluated for chemical composition. All three samples met the 99.5 pure zinc requirement of the ASTM B6 standard[14] prescribed for the original socket castings. Tensile tests were performed on 10 zinc coupons, and the ultimate tensile stress ranges from 3 ksi to 12 ksi depending on the coupon

[13] American Society for Testing and Materials (ASTM). *ASTM A586-18. Standard Specification for Metallic-Coated Parallel and Helical Steel Wire Structural Strand.* 2018.

[14] American Society for Testing and Materials (ASTM). *ASTM B6-18. Standard Specification for Zinc.* 2018.

locations. The coupons extracted near the front of the casting (smaller diameter end) had a higher ultimate tensile stress than the coupons taken near the back of the casting (larger diameter end). This is consistent with the distribution of grain sizes in the casting. A smaller grain size was observed at the front of the sockets and is likely due to faster cooling of the zinc during the socketing process. In the casting of an auxiliary socket, it was also observed that the galvanizing zinc had not been removed from the wires prior to socketing. Details of the tests performed on the zinc castings are provided in Appendix M.

3.3.3 Socket Wire Broom Geometry

During socketing, the cable's wires are spread out inside the socket to form a broom before pouring zinc. The casting of socket M4-4_T (second cable failure) and four auxiliary sockets (M8N_T, B4N_G, B4S_G, B12W_G) that exhibited different degrees of cable slip were cut in the transverse direction to observe the wire broom. As shown in Figure 32, the wire brooms are irregular, and differences in wire distribution between the center and perimeter of the casting can be observed. Additional observations and results on the wire broom geometry are provided in Appendix M.

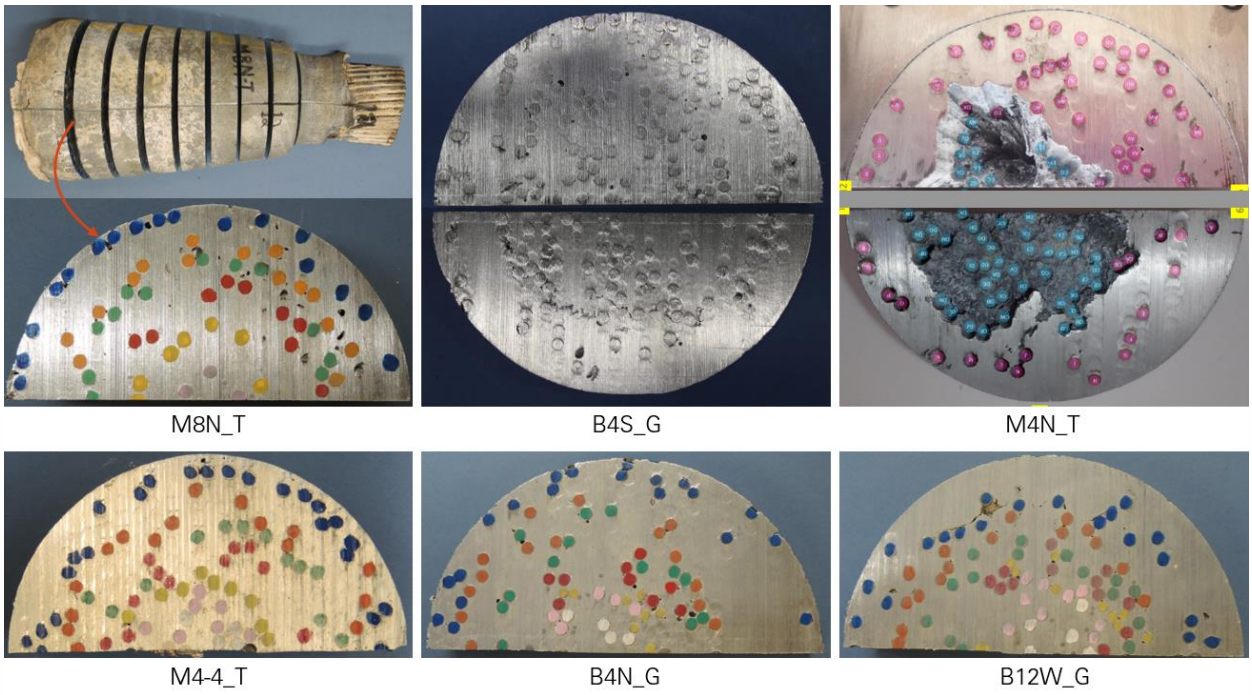

Figure 32: Wire distribution at back of socket castings *(M4N_T photos: WJE[15]; other photos: Socotec).*

3.3.4 Socket Failure Mechanism

The zinc casting of sockets that failed or experienced significant cable slips were cut open longitudinally, and three key features were observed (Figure 33). First, a displaced inner core was observed within the casting of every socket. This core is shaded in Figure 33 for illustration and can be approximated as a cylindrical volume centered on the socket's axis and with a diameter equal to the smaller diameter of the

[15] Wiss, Janney, Elstner Associates (WJE). *Auxiliary Main Cable Socket Failure Investigation*. June 21, 2021. Draft report provided by WJE.

socket's cavity. Second, ruptured outer wires were observed in the sockets that failed. And third, outer wires were observed to have slipped within the zinc outside of the displaced core in the socket that exhibited the largest cable slip but did not fail (B12W_G).

The surfaces of the longitudinal cuts of the socket's castings were macro-etched to observe the grain structure. Elongated deformation of the zinc grains was observed between wires near the surface of the displaced casting core (Figure 34).

The inner core and the inner wires completely pulled out of the first socket that failed (M4N_T). In the second socket that failed (M4-4_T), the core remained in the socket after shifting significantly and the remaining wires ruptured outside of the core. As a result, the two failed sockets look different yet both failures started inside the socket with a displacement of the core and the rupture of outer wires (Figure 35).

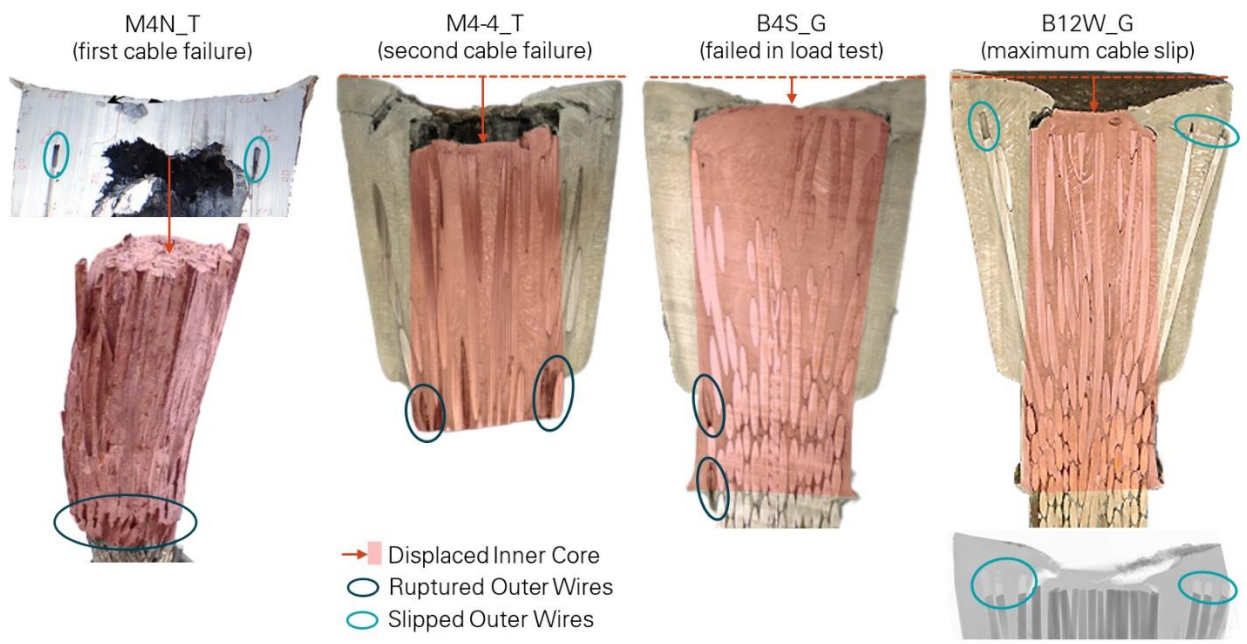

Figure 33: Observations in distressed sockets *(M4N_T photos: WJE[16]; B12W_G radiograph: Adrian Brügger, Columbia University - Oak Ridge National Laboratory; other photos: Socotec).*

[16] Wiss, Janney, Elstner Associates (WJE). *Auxiliary Main Cable Socket Failure Investigation.* June 21, 2021. Draft report provided by WJE.

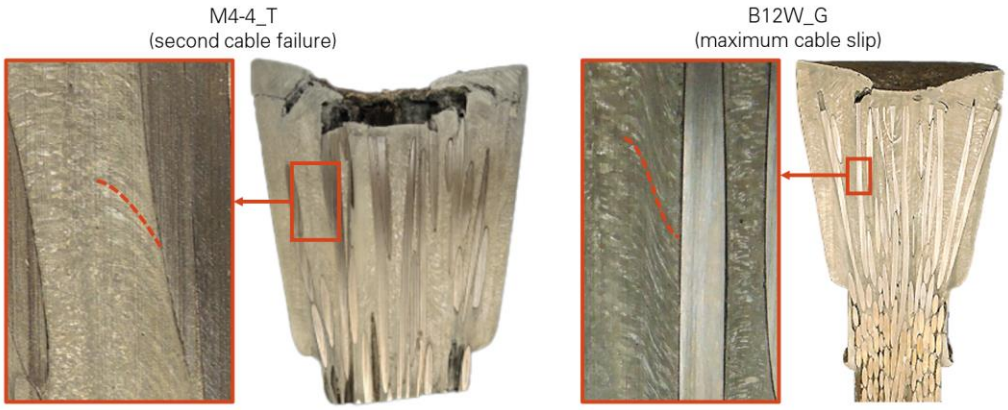

Figure 34: Evidence of grain flow near surface of displaced core in socket zinc casting *(photos: Socotec).*

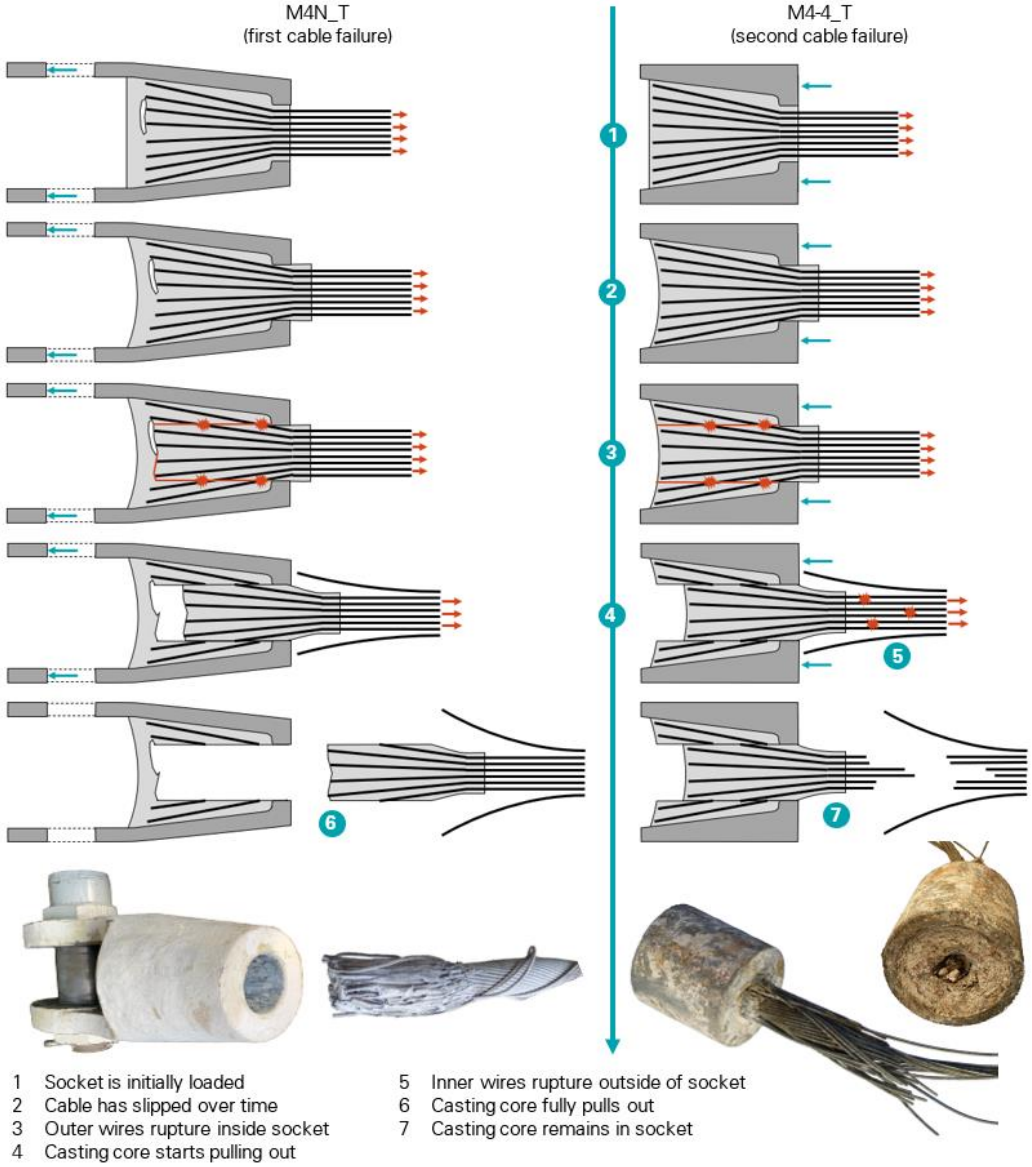

Figure 35: First two socket failures
(M4N_T socket photo: NAIC Arecibo Observatory, a facility of the NSF; M4-4_T photos: Socotec).

4.0 Analysis

A set of analyses was performed on mathematical and digital models of the telescope and sockets to interpret the field and laboratory observations and further investigate the socket failures. The forces in the sockets during telescope operation and extreme environmental events, such as hurricanes and earthquakes, were determined first. The sockets' behavior and failures under those forces were then analyzed.

4.1 Socket Force Analysis

The forces in the telescope's sockets were determined through analysis of the entire telescope structure under a variety of loads representing the telescope's typical conditions and extreme environmental events. The objective was to determine the maximum forces that the cable sockets experienced in each condition, along with the amplitude and frequency of the force cycles.

4.1.1 Method and Assumptions

The cable tensions were determined using finite element (FE) analysis models of the original and upgraded telescope structure (Figure 36). The models include the telescope's suspended structure, towers, waveguide, and the main, backstay and tiedown cables. The Gregorian and line feed(s) are modeled as loads on the suspended structure, and the cables are modeled as special tension-only elements that capture the cable's sag and associated stiffness reduction. The cable properties are modeled per the ASTM A586 standard prescribed for the telescope's cables. For the towers, the concrete properties are based on test results of concrete cores taken from the towers after the collapse. Additional information on the analysis models is provided in Appendix F.

The sockets transfer the cable tensions to the telescope's platform, towers, and anchorages. The socket forces are therefore equal to the cable tensions obtained from the FE models. Since the main and backstay cables are inclined, the tension is slightly different at the two ends of each cable. However, because the cables are highly tensioned, the relative difference in tension between the ends of any cable is less than two percent. This difference is considered by reporting the average cable tension over the length of the cable.

No design capacity is known for the sockets of the telescope. Spelter sockets are typically expected to develop the full Minimum Breaking Strength of the connected cables based on proof load tests by the cable manufacturers. As a measure of the stress level in a cable and the connected socket, the cable's safety factor (SF) is used in our analysis. As noted earlier, the safety factor is defined as the ratio of the cable's Minimum Breaking Strength to the cable's actual tension. The normalized stress range (NSR) is used to evaluate how much a cable's tension fluctuates under operational loads and temperature, wind, and seismic effects. The normalized stress range is defined as the ratio of the cable's peak-to-peak tension change to the cable's Minimum Breaking Strength.

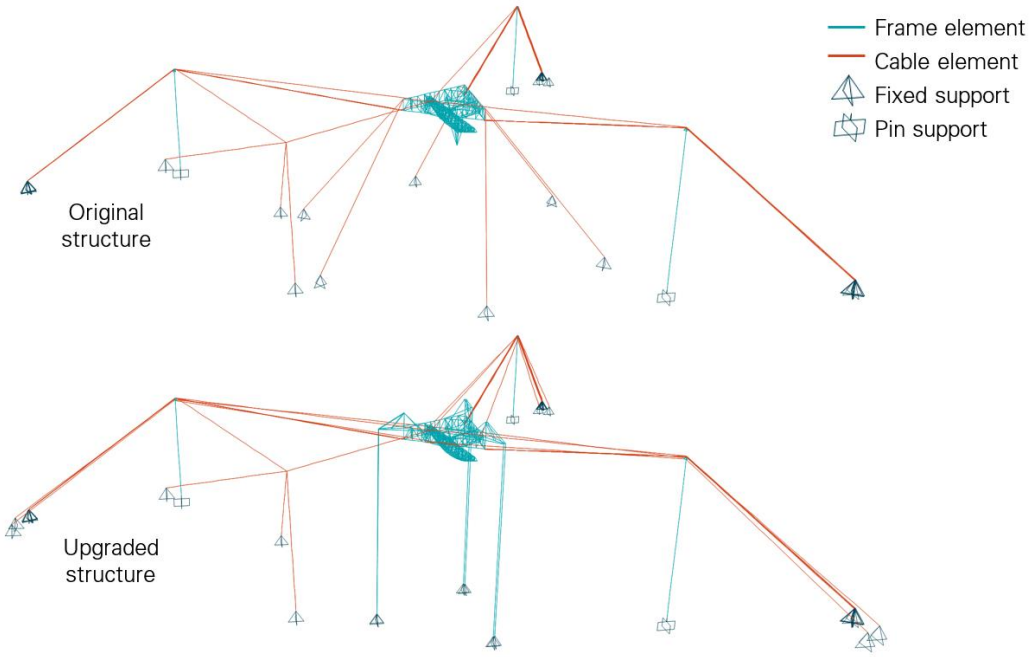

Figure 36: FE models of original and upgraded telescope structure.

4.1.2 Analysis of Typical Conditions

For the majority of its lifetime, the telescope was primarily subjected to three load effects: its own weight, the movement of the azimuth arm, Gregorian and line feed(s) during operation, and the day-night temperature cycle.

Telescope Weight

The weight of the original and upgraded structures, respectively 1,225 kip and 1,825 kip, is considered in the analyses. Before applying any additional load (seismic, wind, etc.), the FE model is initialized in a baseline state where the cable tensions under the structure's weight are known. For the original structure, the baseline tensions are the cable tensions determined by AW before the second upgrade. To determine the baseline tensions in the upgraded structure, we used the cable sag survey performed in August 2020 after the first cable failure, and we removed the effect of the cable failure through analysis. This process is detailed in Appendix G.

Telescope Operation

To simulate the movement of the azimuth arm, Gregorian and line feed during operation of the upgraded telescope, we applied moving loads on the fixed platform in the FE model. The maximum changes in cable tension due to telescope operation were determined by simulating a full rotation of the azimuth arm with the Gregorian fully extended out and the line feed pointing straight down, which maximizes the load imbalance on the fixed platform. Results are shown in Figure 37 for representative auxiliary cables, and the largest normalized stress range due to telescope operation is 3.8 percent. We also simulated multiple days of actual telescope operation based on logs of the azimuth arm, Gregorian and line feed positions. From the simulation results, the number and magnitude of the cable tension cycles were determined statistically. The number of cycles is in the order of five cycles per day during standard

telescope operation, and 90 cycles per day when the telescope is used for atmospheric studies. In both cases, the maximum normalized stress range is less than four percent. The telescope operation analysis is detailed in Appendix H.

Temperature Cycles

On an average night, the total tension in the tiedowns of the upgraded structure increases by 60 kip as jacks pull down on the tiedowns to keep the platform at a constant elevation (Figure 38). From the FE model, we determined that the platform elevation remains constant under the additional tiedown tension if the temperature of the platform and cables decreases by 15.8°F. This result is consistent with the 12.3°F average day-night temperature difference measured in the air on the telescope's platform. The combined effect of the additional tiedown tension and temperature drop is a three percent increase in the main and backstay cable tensions. We applied the same 15.8°F temperature drop to the FE model of the original structure, and observed a 2.5 percent increase in cable tensions. For both structures, these fluctuations correspond to normalized stress ranges of less than two percent. The temperature analysis is detailed in in Appendix I.

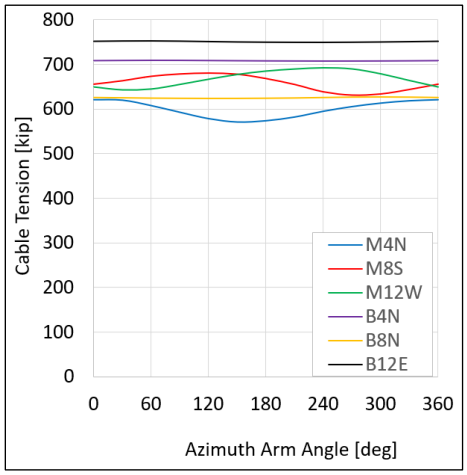

Figure 37: Tension in representative auxiliary cables during full revolution of azimuth arm with Gregorian fully extended out.

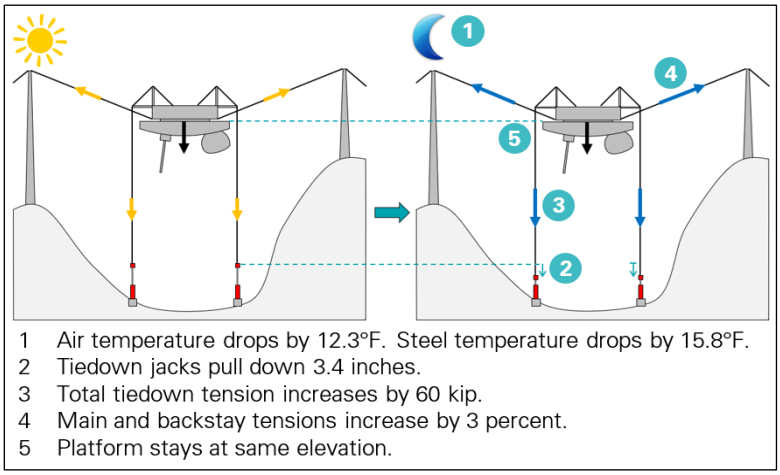

Figure 38: Impact of average day-night temperature cycle on upgraded telescope structure.

4.1.3 Analysis of Extreme Environmental Events

The loads induced by windstorms and earthquakes are transient, and their effect on the telescope was determined through dynamic analysis in the FE models. The telescope's structure tends to respond dynamically according to its fundamental modes of vibration, which combine movement of the platform and bending of the towers. The first modal period is 2.3 seconds for the original structure, and 3.0 or 4.5 seconds for the upgraded structure depending on whether the tiedowns are taut or released. We considered a damping ratio of one percent for the structure's global modes, which we estimated from the vibrations recorded in the tiedown tensions during the first cable failure. The structure's modal properties are detailed in Appendix F.

Windstorms

To determine the sustained and turbulent loads induced by wind on the telescope's platform, we performed a series of computational fluid dynamics (CFD) analyses (Figure 39). The results were then calibrated with actual wind speed time histories recorded on the platform, and applied to the FE models of the telescope. Through this process, we simulated the structure's response to 2.5 hours of typical ambient wind, and to the 2.5 hours leading up to the peak of Hurricane Maria.

Ambient wind causes a normalized stress range of less than one percent in the cables, with approximately 28,000 cycles per day. In the wind conditions of Hurricane Maria, the most significant wind gusts result in a normalized stress range of up to four percent in the original structure, and eight percent in the upgraded structure. The impact is more significant in the upgraded structure primarily because of the down-drag wind force acting on the Gregorian. The impact of Hurricane Maria on some of the cables of the upgraded structure is shown in Figure 40. The wind analysis is detailed in Appendix J.

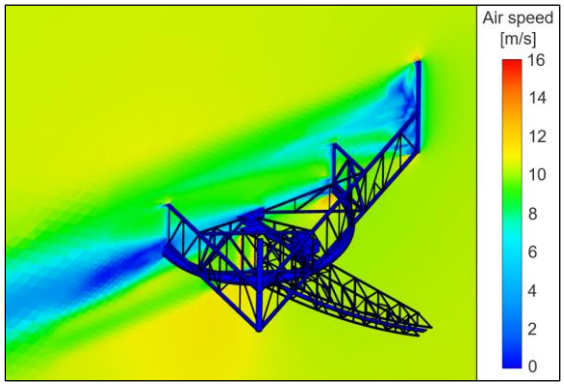

Figure 39: Computational fluid dynamics analysis of platform for 10 meter per second (22.4 mph) wind.

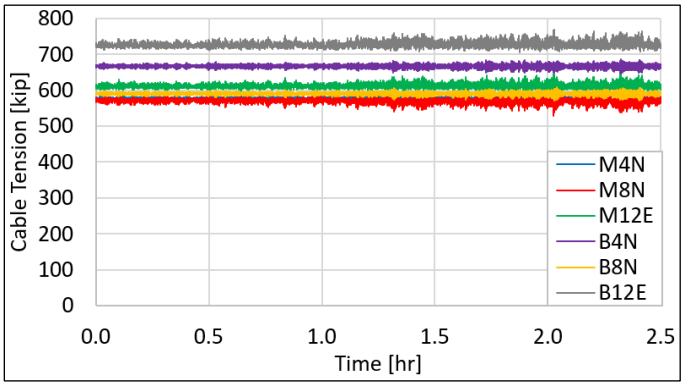

Figure 40: Tension in representative auxiliary cables during peak of Hurricane Maria.

Earthquakes

To evaluate the potential impact of seismic activity on the cable tensions, we analyzed the telescope's response to two significant earthquakes that occurred in January 2020 and the ground accelerations of which were recorded at the Observatory. The response spectrum for the larger earthquake, of moment magnitude 6.4, is shown in Figure 41. The response spectrum indicates that the earthquake primarily affects stiffer structures with periods shorter than one second, while the telescope's first global modes have periods greater than two seconds. In the FE models, we applied the recorded ground accelerations with a time delay between the different towers and cable anchorages based on the estimated shear wave velocity at the site. Considering both earthquakes and a range of shear wave velocities, the maximum normalized stress range is eight percent in the original structure and five percent in the upgraded structure. The impact of the larger earthquake on some of the cables of the upgraded structure is shown in Figure 42. The earthquake analysis is detailed in Appendix K.

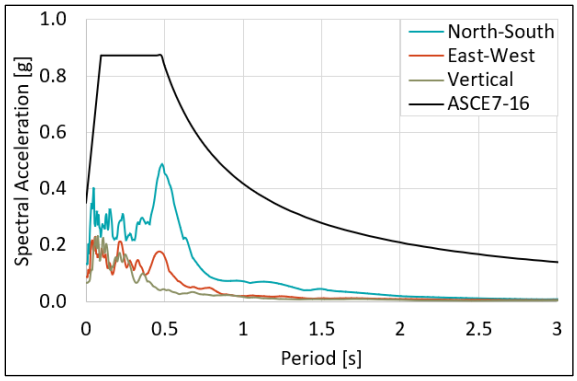

Figure 41: Response spectra of ground accelerations measured at AO during January 7, 2020, M6.4 earthquake, compared to design response spectrum.

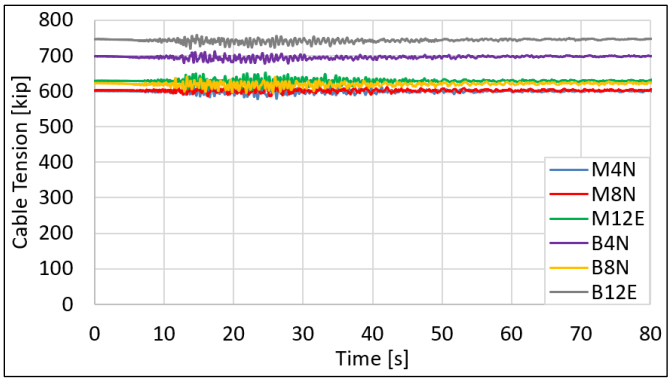

Figure 42: Tension in representative auxiliary cables during January 7, 2020, M6.4 earthquake

4.1.4 Analysis of Cable Failure Events

The two cable failures that occurred before the collapse caused tension redistribution among the remaining cables. We performed an analysis of the cable tensions throughout the 2020 events, and the results for the main cables are summarized in Figure 43 (cable tensions) and Figure 44 (cable safety factors).

The cable tensions were first measured on site by surveying the cable sags when the telescope was stowed after the first cable failure (M4N). Starting from these known tensions in the FE model, we simulated the cable failures and telescope movements that occurred before and after the sag survey.

By comparing the position of the platform before and after the first cable failure (M4N), we determined that cable M4N carried a tension of 600 kip when it failed. This corresponds to a safety factor of 2.2. The M4N failure had a significant impact on the four original M4 cables, decreasing their safety factor from 2.0 to 1.6. After one of these cables failed (M4-4), the safety factor of the remaining three M4 cables dropped to 1.3. The collapse started with the failure of another M4 cable (M4-2). If the structure had stabilized after this third cable failure, the safety factor in the remaining two M4 cables would have been less than 1.0.

The M4N failure had a more significant impact on the redistribution of cable tensions than the M4-4 failure. Since M4N was an isolated cable, its failure resulted in an imbalance in the suspended structure. The suspended structure rotated to reach a new balance state resulting in increased and decreased tensions in the rest of the cable system. M4-4 ran in parallel with three other original M4 cables. As a result, when M4-4 failed, its tension was primarily redistributed to the three other M4 cables.

The impact of the 2020 events on the cable tensions is detailed in Appendix G.

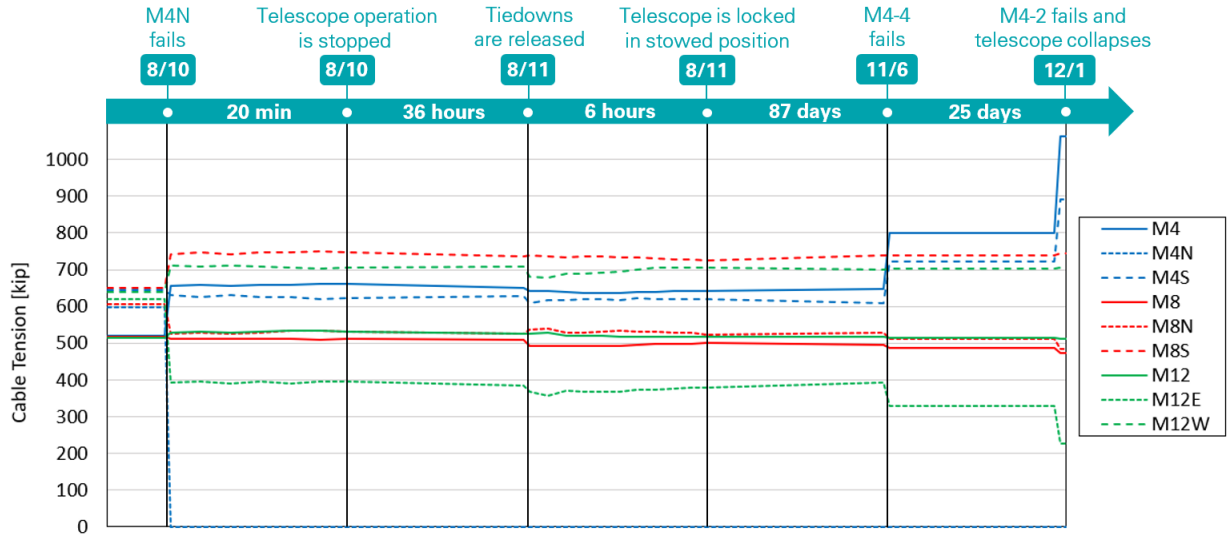

Figure 43: Tension in main cables between first cable failure and collapse.

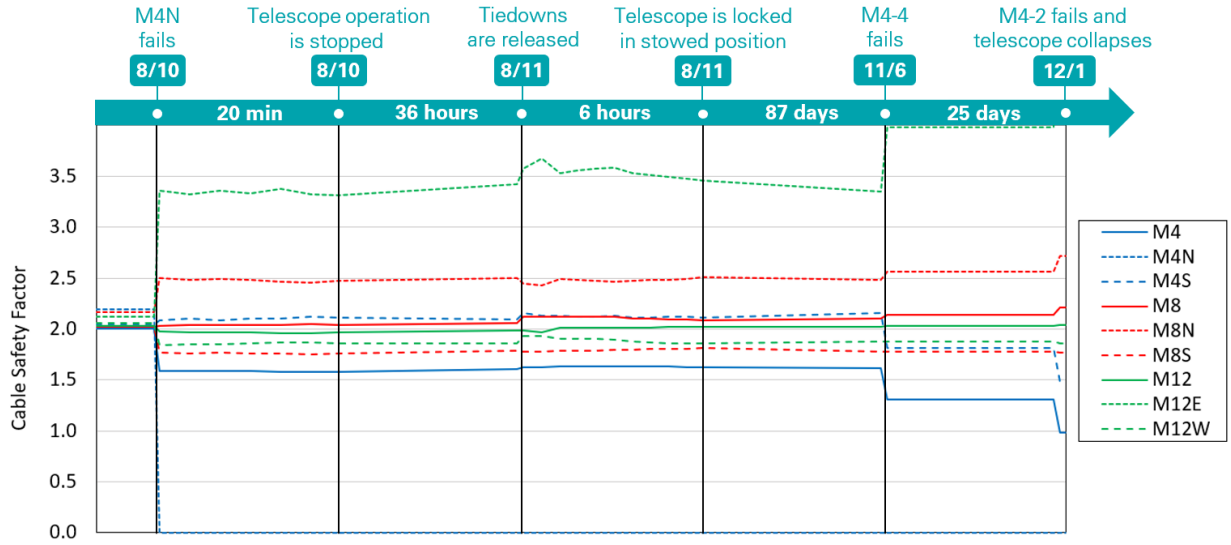

Figure 44: Safety factor in main cables between first cable failure and collapse.

4.1.5 Summary

The safety factors and normalized stress ranges under different loading conditions are summarized in Table 4 for the cables that failed prior to collapse (M4, M4N), the cable where the maximum slip was observed at a socket (B12W), and the average of all mains and backstays. For transient loading conditions (telescope operation, Hurricane Maria, and 2020 earthquakes), the safety factor is calculated based upon the maximum cable tension experienced. Every loading condition includes the weight of the telescope.

The results show that before and after the second upgrade, the safety factors were not significantly affected by the telescope operation or the wind and seismic events. The cable failures in 2020 reduced the safety factors in the M4 cables from 2.1 to as low as 1.3 because the tension in the remaining cables

increased after the first two cables failed. The safety factor in cable B12W, whose ground-end socket exhibited the largest cable slip, was 17 percent higher than that in the average backstay. The normalized stress ranges during transient loading conditions are under seven percent, which is not large enough to cause a fatigue issue.

Table 4: Minimum safety factor (SF) and normalized stress range (NSR) in selected cables and on average over all main and backstay cables

		Cable M4[A]		Cable M4N[B]		Cable B12W[C]		Average Main		Average Backstay	
		SF	NSR	SF	NSR	SF	NSR	SF	NSR	SF	NSR
Before Second Upgrade	Telescope Stowed	2.1	-	-	-	-	-	2.1	-	2.3	-
	Temperature Cycle	2.1	1.2%	-	-	-	-	2.1	1.2%	2.3	1.1%
	Telescope Operation	2.1	0.0%	-	-	-	-	2.1	0.0%	2.3	0.0%
	Hurricane Maria[D]	1.9	4.0%	-	-	-	-	1.9	4.1%	2.1	3.7%
	2020 Earthquakes[D]	2.0	2.6%	-	-	-	-	2.0	4.4%	2.2	5.0%
	Worst Combination[E]	1.9	-	-	-	-	-	1.9	-	2.1	-
After Second Upgrade	Telescope Stowed	2.0	-	2.2	-	2.6	-	2.0	-	2.2	-
	Temperature Cycle	1.9	1.6%	2.2	1.2%	2.5	1.2%	2.0	1.5%	2.2	1.3%
	Telescope Operation	1.9	1.9%	2.1	3.8%	2.6	0.2%	1.9	2.5%	2.2	0.1%
	Hurricane Maria	1.9	6.0%	2.1	4.9%	2.5	3.8%	1.9	6.5%	2.1	5.0%
	2020 Earthquakes	1.9	3.9%	2.1	3.4%	2.5	2.8%	1.9	3.8%	2.1	2.9%
	Worst Combination[E]	1.8	-	2.0	-	2.4	-	1.8	-	2.0	-
After First Cable Failure	After M4N Failure	1.6	-	-	-	2.7	-	2.0	-	2.3	-
	After M4-4 Failure	1.3	-	-	-	2.7	-	2.0	-	2.3	-
	After M4-2 Failure[F]	1.0	-	-	-	2.7	-	2.2	-	2.4	-

[A] M4 is a set of four cables including M4-4 (second cable to fail) and M4-2 (third cable to fail, triggering collapse).
[B] Cable M4N is the first cable to fail.
[C] The largest cable slip was observed at the ground-end socket of cable B12W.
[D] This event occurred after the second upgrade but is used as representative extreme event for analysis.
[E] Worst case between (operation + earthquake) and Hurricane Maria.
In both cases, the temperature is assumed to be 10°F lower than the daytime average.
[F] Static analysis, assuming that structure stabilized after M4-2 failure.

4.2 Socket Strength Analysis

Three of the telescope's sockets failed and other sockets showed significant cable slip while the tension in the connected cables was less than their Minimum Breaking Strength. We investigated the cable slips and socket failures through calculations, finite element analysis, and a full-scale load test to failure. The socket behavior inferred from our investigation is presented first, followed by the supporting analyses.

4.2.1 Socket Behavior

In a zinc-filled spelter socket, the cable tension is transferred to the socket through a zinc casting. In the telescope's sockets that failed or exhibited the largest cable slip, we observed the displacement of a cylindrical *core* within the casting. If we consider the forces acting on this core (Figure 45), the cable tension is resisted by shear stress on the core surface and/or tension in the wires that cross through the

core surface. These wires are referred to as the *crossing wires*, and are typically part of the outer layers of the cable.

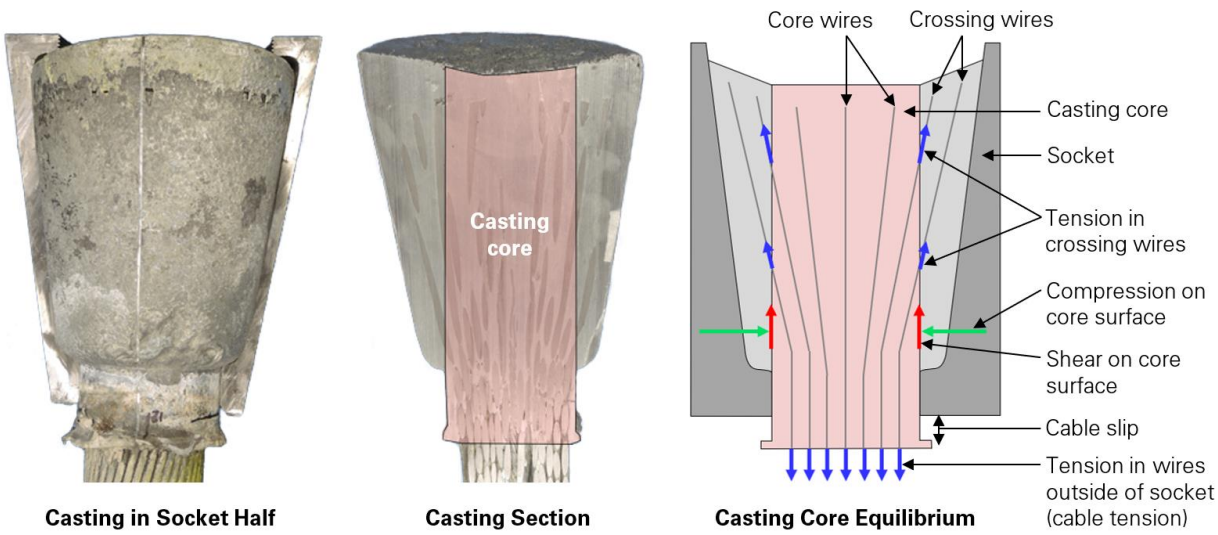

Figure 45: Equilibrium of socket casting core *(photos: Socotec).*

The cable slips observed on the telescope's sockets are the result of two mechanisms. First, the pre-stretching and/or initial loading of the cable caused the zinc casting to shift and deform to become tightly wedged into the socket. This is expected to occur in any zinc-filled spelter socket, and to result in a relatively small cable slip (up to one sixth of the cable diameter per AASHTO[17]). In the telescope's sockets that were cut open, we observed that the cable slip had increased due to a displacement of the casting's core. This second mechanism caused the large cable slips observed on the telescope's sockets, and is the focus of our analysis.

For the core to displace within the casting, a compatible shear movement must occur between the core and the rest of the casting. This movement may occur through plastic deformation or creep of the zinc near the core surface, which we refer to as *zinc flow*. Zinc flow can only occur if a shear stress is acting on the core surface. In other words, the core cannot displace when the full cable tension is resisted by the crossing wires, such that there is no shear stress on the core surface.

A key parameter affecting the cable slip is therefore the wire broom geometry, which includes the number of crossing wires, their length outside of the core, and their orientation with respect to the core surface. If a cable was not broomed out, the cable tension could only be resisted in shear on the core surface (Figure 46). This would result in rapid zinc flow, zinc shear failure and/or cable slip from the zinc. In any case, the cable would slip out of the socket under any substantial tension. Conversely, when the cable is broomed out, the crossing wires stretch and pick up more tension as the cable slips due to zinc flow (Figure 47). The increased tension in the crossing wires decreases the shear stress on the core, which slows down and effectively stops the zinc flow and cable slip. This, however, is only possible if the crossing wires have a sufficient capacity collectively to resist the full cable tension.

[17] American Association of State Highway and Transportation Officials (AASHTO). *AASHTO M 277-06. Standard Specification for Wire Rope and Sockets for Movable Bridges*. 2019.

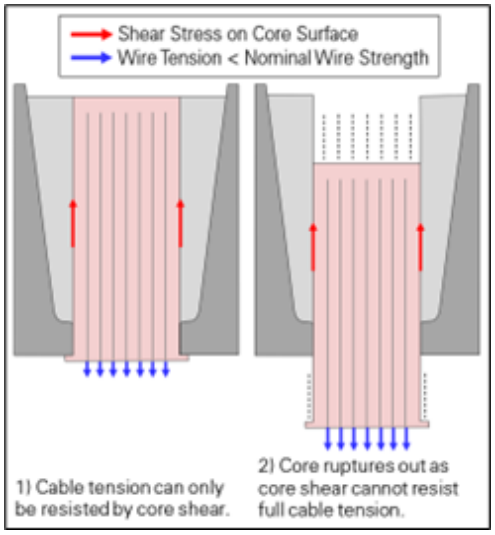

Figure 46: Case 0 – Core rupture in absence of wire broom.

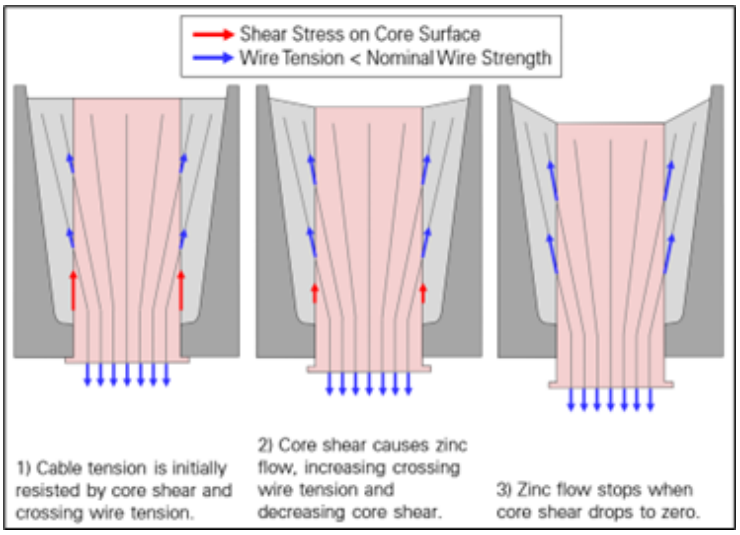

Figure 47: Case 1 – Limited cable slip when crossing wires can resist full cable tension.

The tensile behavior of a steel wire is elastoplastic and simplified as elastic-perfectly plastic in the following to describe socket behavior. The maximum tension that a wire can resist before yielding and eventually rupturing is referred to as the *nominal wire strength*. A crossing wire is considered *fully developed* if its bond and friction with the zinc outside of the core is sufficient to resist the nominal wire strength without slipping. Conversely, a crossing wire that slips outside the core under a tension lower than the nominal wire strength is considered *partially developed*.

A socket where the crossing wires cannot resist the full cable tension is bound to fail, and the socket's failure mode depends on whether the crossing wires are fully or partially developed. If the crossing wires are fully developed (Figure 48), they continue to stretch near the core surface as the zinc continues to flow. Some of the wires rupture when they reach their ultimate tensile strain, which increases core shear and accelerates zinc flow, leading to more wire ruptures and, eventually, to *core rupture*. If the crossing wires are partially developed, they can slip in parallel with the core instead of rupturing, leading to *core flow-out* (Figure 49). In this case, the cable continues to gradually slip out of the socket. Complete slip-out or rupture of the core will eventually occur as the contact length between cable and socket decreases and/or the zinc's strain becomes too large. Macroscopically, the socket failure is more brittle when the crossing wires are fully developed, and more ductile when the crossing wires are partially developed. Actual sockets may include both fully and partially developed crossing wires and therefore exhibit intermediate behaviors and failure modes (Figure 50).

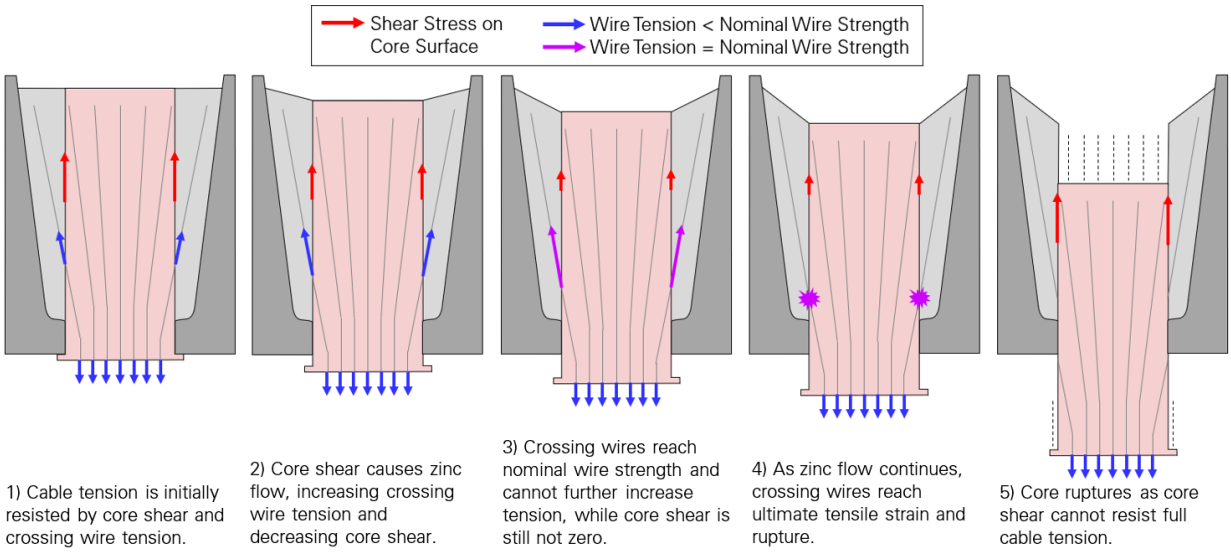

Figure 48: Case 2 – Core rupture when crossing wires cannot resist full cable tension and are fully developed.

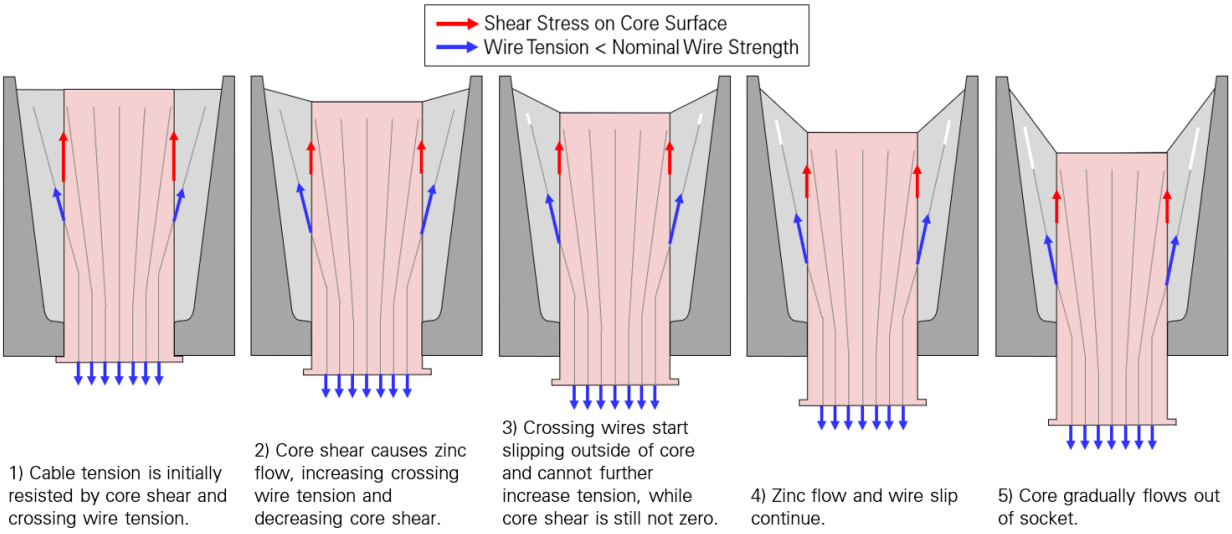

Figure 49: Case 3 – Core flow-out when crossing wires cannot resist full cable tension and are partially developed.

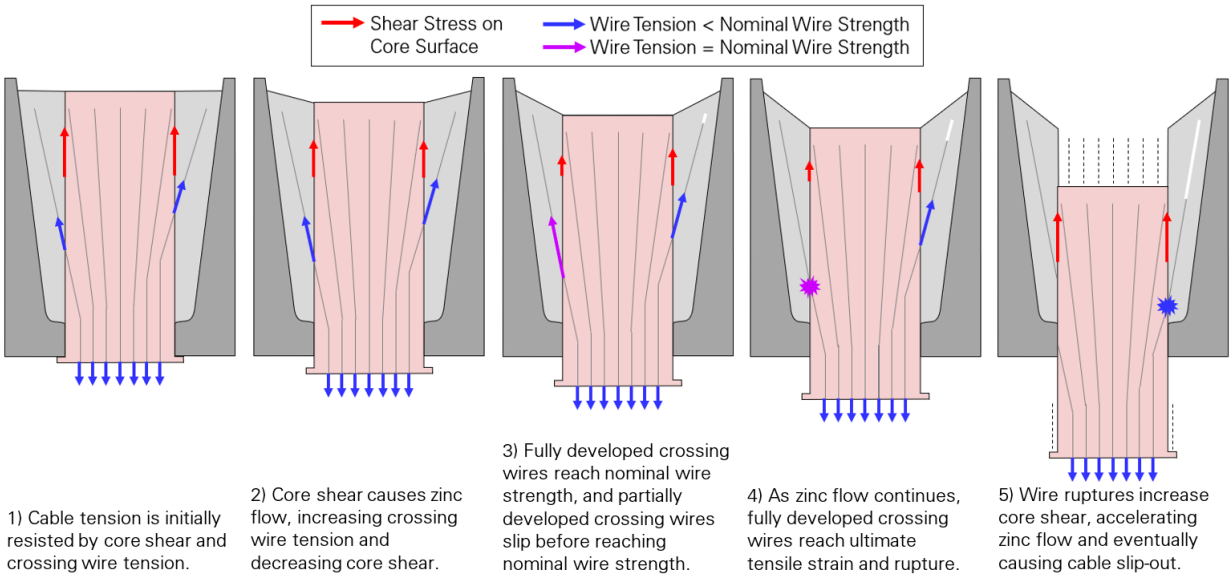

Figure 50: Case 4 – Socket failure when crossing wires cannot resist full cable tension and include both fully and partially developed wires.

4.2.2 Finite Element Analysis

The socket behavior presented above is consistent with the results of a series of analyses performed on finite element (FE) models of zinc-filled spelter sockets. The models and results are summarized in the following, and detailed in Appendix P.

Model

The baseline FE model represents an auxiliary backstay ground-end socket with a uniform wire broom, where the wires are evenly spaced in the radial and circumferential directions (Figure 51). Such wire broom has a 60-degree axisymmetry, and therefore the model is limited to a 60-degree wedge with appropriate boundary conditions. The zinc casting can overcome friction and slip on the surface of the socket cavity. The zinc is modeled as an elastoplastic material based on laboratory tensile test results, and assigned a creep behavior allowing the material to continue to deform under sustained tensile or shear stress. The wires' steel is also modeled as an elastoplastic material based on the laboratory tensile test results. The wires are tied to the zinc, i.e. wire slip within the zinc is not modeled.

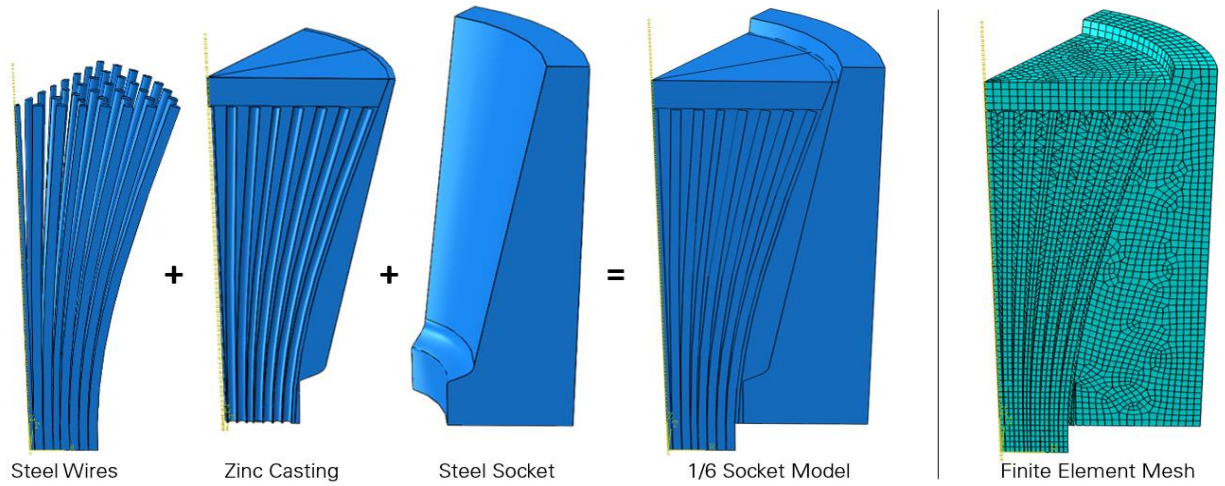

Figure 51: Baseline FE model of auxiliary backstay ground-end socket.

Effect of Socket Shoulder

The baseline model represents a socket whose design includes a shoulder, like all of the telescope's sockets that failed or exhibited large cable slips. To study the effect of the shoulder on socket behavior, a FE model was constructed by removing the shoulder from the baseline model. After loading both models to half of the cable's breaking strength, the load was held to allow the zinc to flow.

The initial loading causes higher shear stress at the front of the zinc casting, as the load is partially resisted in bearing on the shoulder (Figure 52). However, after one year of zinc flow, the shear stress distribution is similar in the castings with and without a shoulder. The wire stresses are also similar in the two models.

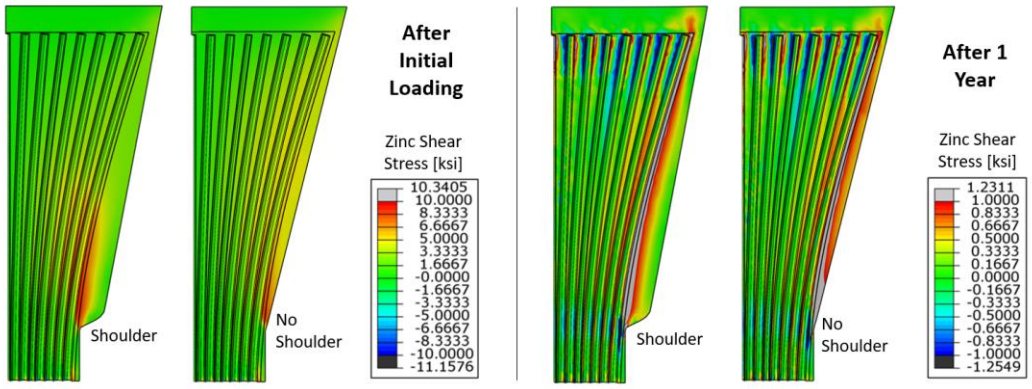

Figure 52: Shear stress in zinc casting with and without shoulder.

Impact of Wire Broom

Additional FE models were derived from the baseline model to study the impact of wire broom geometry on socket behavior. These include models where only one, two and three layers of wires are broomed out, and a model where the wire broom is uniform but narrower than in the baseline model (Figure 53).

The models were loaded to half of the cable's breaking strength, and the load was held while simulating 25 years of zinc flow.

In the cable modeled with the socket, the two outermost wire layers account for 48 percent of the cable's section area. Those two layers are therefore sufficient to resist most or all of the applied load, which is 50 percent of the cable's minimum breaking strength. With that in mind, the FE analysis results (Figure 53, Figure 54) are consistent with the socket behavior previously introduced (Figure 47 vs. Figure 48, pages 34 to 35): if the full cable tension can be resisted by the broomed-out wires (uniform, three-layer and two-layer brooms), zinc flow stops and the socket does not fail and shows limited cable slip. In contrast, if the broomed-out wires cannot resist the full cable tension (one-layer broom), zinc flow and cable slip continue over time and eventually cause the socket to fail. As wire slip within the zinc was not modeled, the wires and the core ruptured in the FE model.

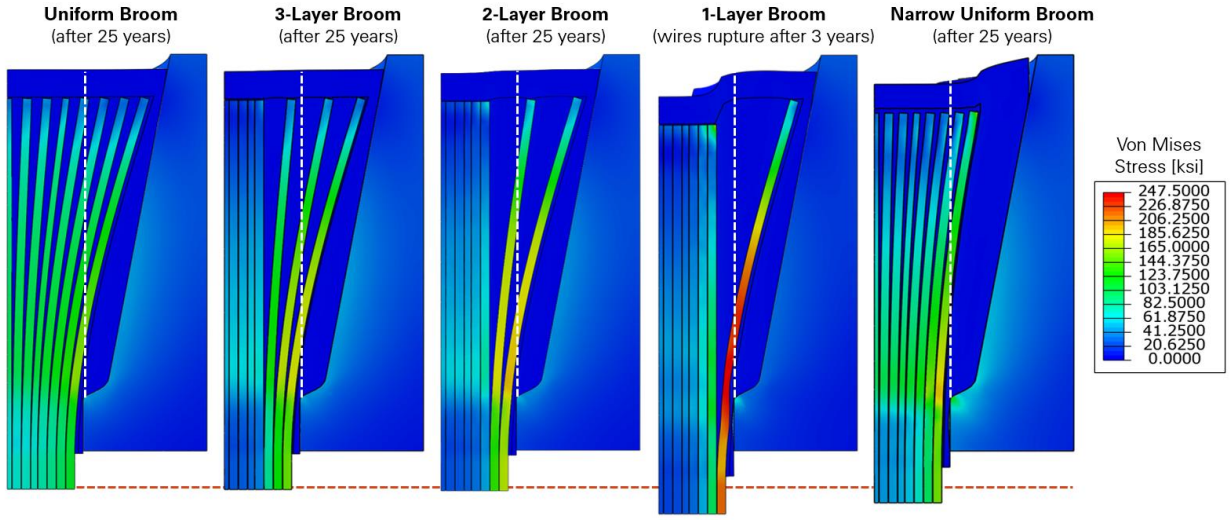

Figure 53: Cable slip and wire stress for different idealized wire brooms after 25 years of zinc flow.

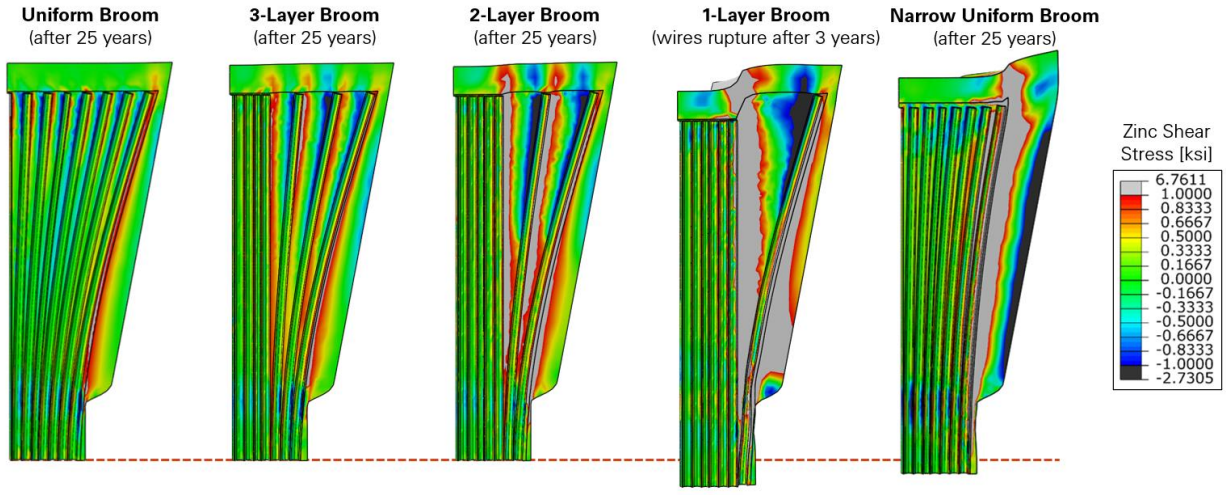

Figure 54: Zinc shear stress for different idealized wire brooms after 25 years of zinc flow.

4.2.3 Socket Load Test to Failure

The recovered ground-end auxiliary backstay socket B4S_G was load-tested to failure at Lehigh University's Fritz Laboratory. The purpose of the test was to observe and measure the behavior of the cable-socket assembly under constant and cyclic loads, and to observe the socket's failure mode.

Socket B4S_G was recovered from the collapsed telescope with 15 feet of cable attached. The socket was generally in good condition, had no visible wire breaks, and exhibited an intermediate cable slip of 0.875 inch. The free end of the cable was cast in a new zinc-filled spelter socket, and the specimen was installed in a test frame (Figure 55).

Over the course of four days, the specimen was initially loaded and held at 100, 125 and 150 percent of the cable's service load of 675 kip for 20 hours, and a series of load cycles was applied at each load level (Figure 57). After unloading to half the service load, the load was increased until seven outer wires ruptured in socket B4S_G (Figure 56) and the specimen was unable to carry more load. The maximum tension reached was two percent greater than the cable's Minimum Breaking Strength, such that the cable still met its design strength requirement after 25 years of service. No wire ruptures were observed at the new socket end.

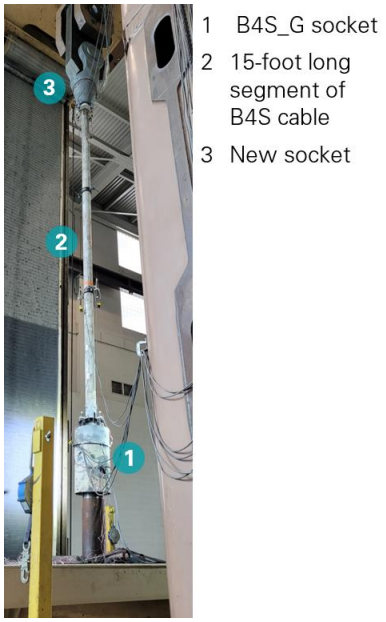

1 B4S_G socket
2 15-foot long segment of B4S cable
3 New socket

Figure 55: Socket and cable specimen in load testing machine.

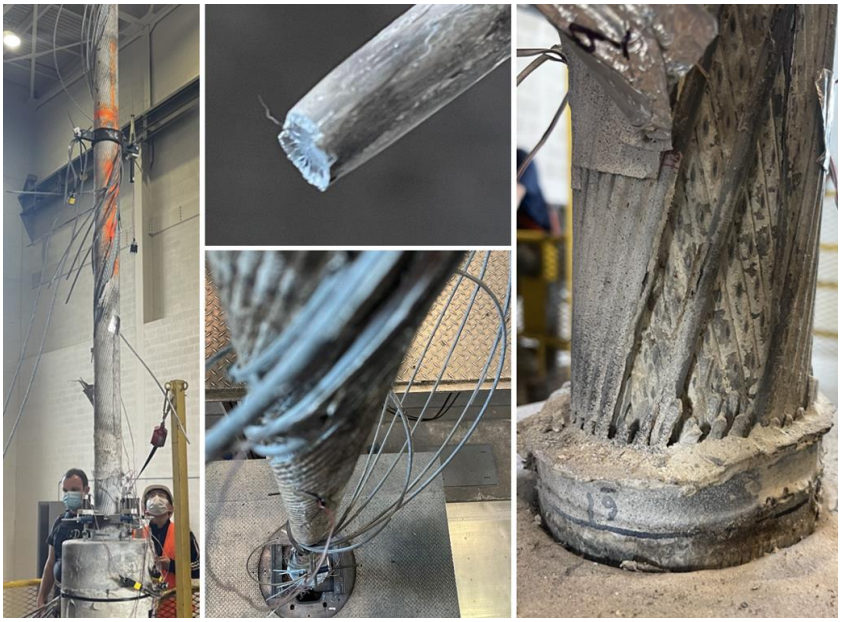

Figure 56: Failed wires in B4S_G socket at end of load test.

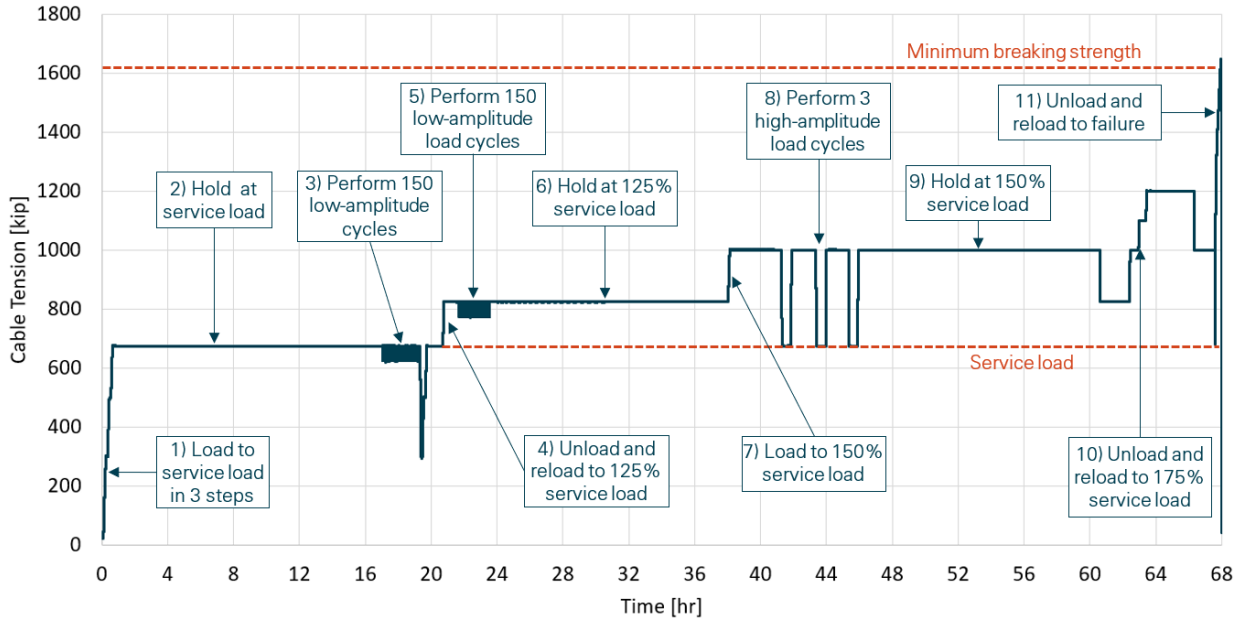

Figure 57: Loading time history of B4S_G socket test.

The zinc flow is non-recoverable, as was observed in the socket load test. The cable slip was monitored throughout the test with four displacement sensors at each socket (Figure 59). Plastic flow occurred in both sockets over the course of each hold, and the flow rate increased with the load. The cable slips resulting from the plastic flow were different between the new and existing sockets, although the cable tension was the same in both sockets. During the initial loading, the cable slip was more than 10 times larger at the new socket (0.35 inch) than at B4S_G (0.03 inch). This is due to the zinc casting of the new socket being wedged into the socket for the first time to achieve load transfer. When the load was increased to the next two levels, the additional cable slip remained larger in the new socket but the difference with B4S_G was less significant. For each load level, the cable continued to slip at both sockets while the load was held constant. This is evidence of time-dependent deformations occurring in the zinc castings. During the final loading to failure, the cable slip increased more at B4S_G (0.40 inch) than the new socket (0.27 inch). Considering the pre-existing slip of B4S_G (0.875 inch), the total cable slip at the end of the test was 1.375 inch at B4S_G, and 0.85 inch at the new socket. This is consistent with the socket behavior previously introduced (Figure 48 page 35), where a socket exhibits significant cable slip before failing. In addition, the total slip of 1.375 inch is relatively close to the last known slip of 1.125 inch at the first telescope socket that failed (M4N_T). The slip rate increased substantially in B4S_G once the cable tension exceeded 75 percent of the Minimum Breaking Strength, and it was clear that the cable was pulling from the socket.

The stress in several outer wires near both sockets was monitored throughout the test with strain gages, while the average cable stress is known from the applied load (Figure 60). Under each increased load, the stress in the outer wires increased disproportionately more than in the inner wires. The outer wire stress is higher than the average cable stress at both sockets, and the difference is generally consistent with the measured cable slip. This is consistent with the socket behavior previously introduced (Figure 47 to Figure 50, pages 34 to 36), where the cable slip causes the tension to increase in the outer wires.

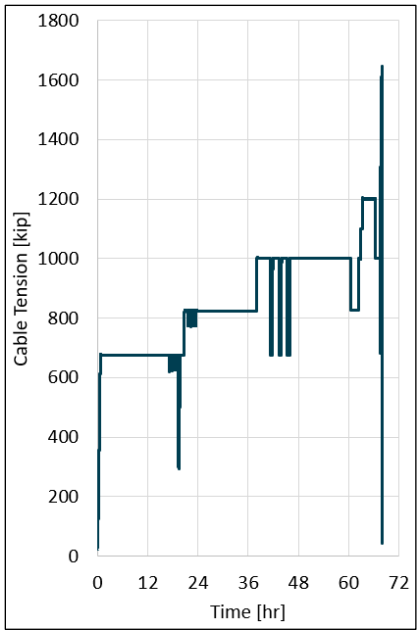

Figure 58: Loading time history.

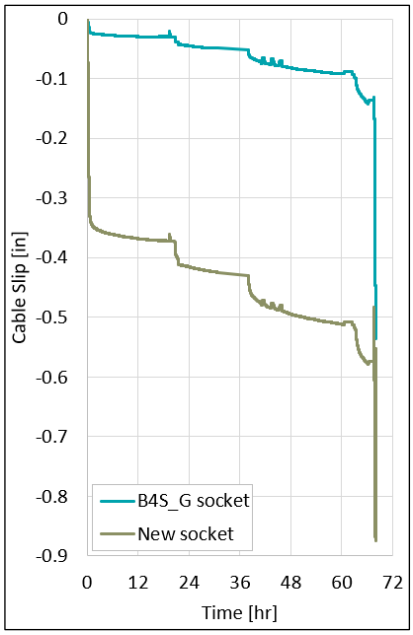

Figure 59: Average cable slip per socket.

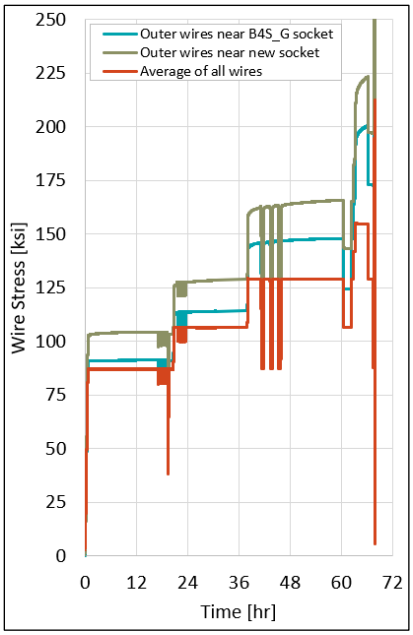

Figure 60: Outer wire stress vs. average cable stress.

4.2.4 Socket Calculations

The socket behavior presented above is consistent with the results of a mathematical model that we developed and applied to the telescope's sockets cut open in laboratories. The model and results are summarized in the following, and additional details are provided in Appendix O.

Model

The proposed mathematical model considers the equilibrium of the socket casting's core (Figure 45 page 33) and calculates the maximum resistance to the cable tension that can be developed in shear on the core surface and in tension in the crossing wires.

The maximum shear resistance is determined according to Mohr-Coulomb theory, based on the cohesion of the zinc material and friction on the core surface. Friction is due to the radial compressive stress induced by squeezing the casting into the cone-shaped socket cavity.

The maximum tensile resistance that a crossing wire can provide is the minimum of the nominal wire strength (fully developed wires) and the wire's slip capacity with respect to the zinc outside the core (partially developed wires). The nominal wire strength is calculated as the average of the yield and ultimate tensile strengths measured on 12 wires taken from the telescope's cables. The wire slip capacity is determined according to Mohr-Coulomb theory, based on the bond strength between wire and zinc, and friction on the wire surface.

Wire Broom Geometry

The wire broom geometry must be known to calculate the capacity of the crossing wires. The wire broom geometry was revealed from transverse cuts in the casting of six telescope sockets (Figure 61,

Figure 62), which include three failed sockets and three other sockets exhibiting different cable slips. The wire broom geometry of socket M4N_T (first cable failure) is provided in WJE's investigation report,[18] and the other five sockets were cut open at Socotec's laboratory.

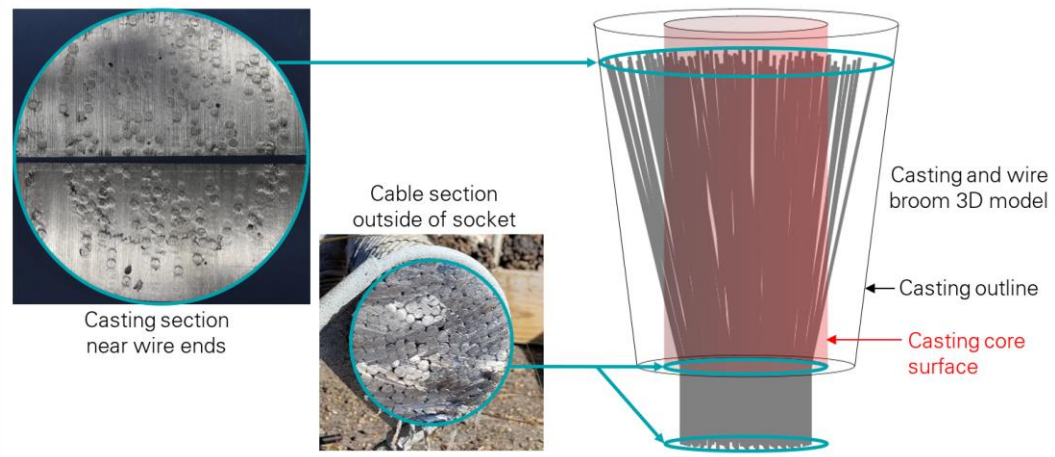

Figure 61: Construction of broom geometry from cable and casting sections *(casting section photo: Socotec).*

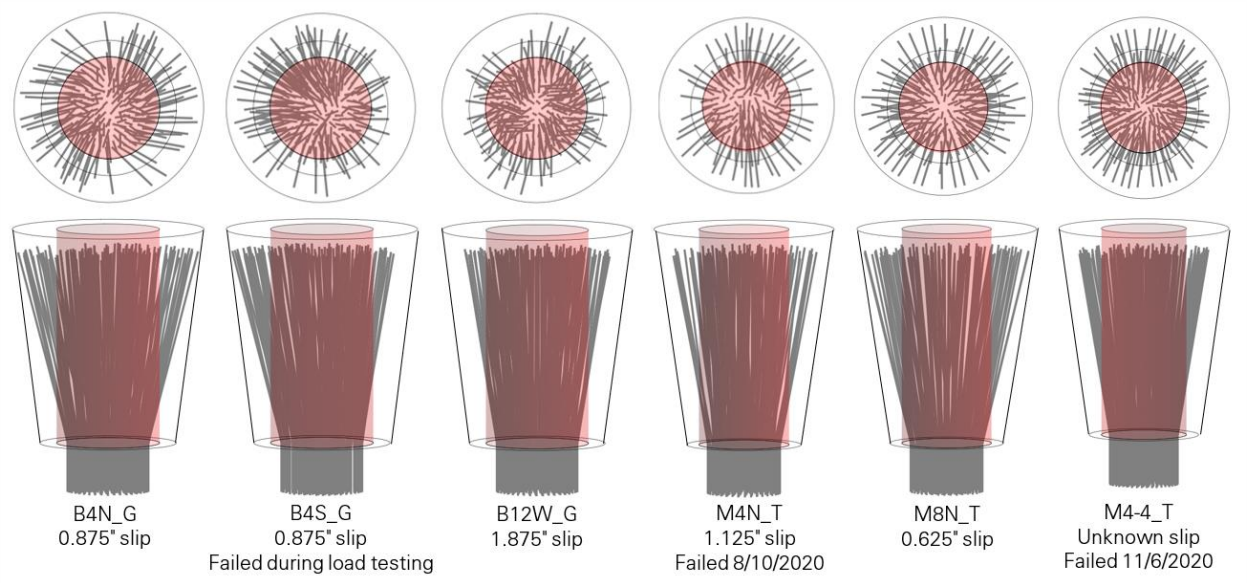

Figure 62: Wire broom geometries considered.

[18] Wiss, Janney, Elstner Associates (WJE). *Auxiliary Main Cable Socket Failure Investigation*. June 21, 2021. Draft report provided by WJE.

To characterize the broom geometry, we define a wire's *brooming ratio* as the wire's distance to the central axis (r) divided by the casting's radius (d) in the plane containing the wire ends (Figure 63). For the five auxiliary sockets considered, the cable slip decreases as the average brooming ratio increases (Figure 64). This result is a first general correlation between wire broom and cable slip, which was further investigated.

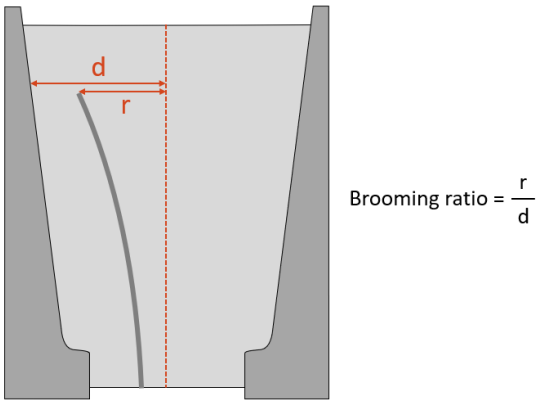

Figure 63: Definition of brooming ratio.

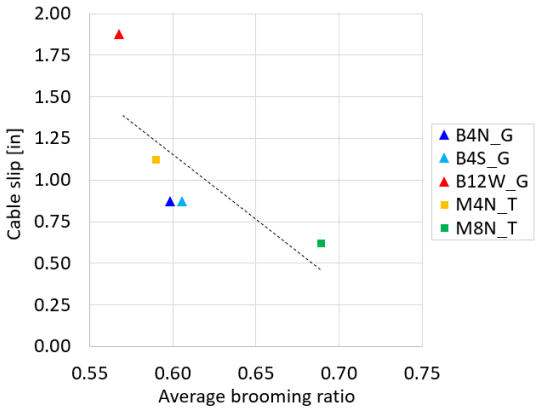

Figure 64: Cable slip vs. average brooming ratio for five auxiliary sockets.

Wire Broom Effect on Cable Slip

For the six sockets of known wire broom geometry, we calculated the minimum shear stress that would be needed on the core surface to resist the cable tension when the crossing wires are loaded to their capacity (Table 5).

Table 5: Required core shear, cable slip and safety factors in sockets considered

		Before M4N Failure						After M4N Failure
		M4-4_T	**M8N_T**	**B4S_G**	**B4N_G**	**M4N_T**	**B12W_G**	**M4-4_T**
Cable Slip [in]		Unknown	0.625	0.875	0.875	1.125	1.875	Visible
Under Gravity Loads	**Cable Tension [kip]**	534	602	665	698	600	624	646
	Crossing Wires Capacity [kip]	565	752	659	671	554	561	581
	Shear Stress Needed on Core [ksi]	0	0	0.05	0.22	0.43	0.52	0.70
	Cable Safety Factor	2.0	2.2	2.4	2.3	2.2	2.6	1.6
Maximum During Hurricane Maria	**Cable Tension [kip]**	543	636	687	721	631	647	-
	Crossing Wires Capacity [kip]	567	761	662	674	558	565	-
	Shear Stress Needed on Core [ksi]	0	0	0.20	0.39	0.69	0.67	-
	Shear Stress Increase vs. Gravity	-	-	+283%	+73%	+58%	+29%	-
	Cable Safety Factor	1.9	2.1	2.3	2.2	2.1	2.5	-
Min. Cable Safety Factor to Not Need Shear Stress on Core		1.8	1.7	2.5	2.4	2.4	3.0	1.8

Under gravity loads, the cable slip increases with the shear stress needed for the five auxiliary sockets (Figure 65 left). In addition, when the first cable failed, the shear stress needed in socket M4-4_T increased from zero to the largest stress (0.7 ksi) among all considered sockets as the M4 cables experienced a 30 percent increase in tension. Socket M4-4_T failed three months later, and fracture

planes were observed around the casting core in the recovered socket. Core movement was also visible on the back of the M4-4_T casting after the first cable failure.

The shear stress needed on the core surface was also calculated for the maximum cable tensions experienced during Hurricane Maria. For the sockets that already relied on the shear stress under gravity loads, the required shear stress increased significantly during the hurricane.

These results are consistent with the socket behavior previously introduced (Figure 47 vs. Figure 48, Figure 49 and Figure 50, pages 34 to 36): the cable slip is driven by the need to transfer the cable tension out of the casting core in shear due to insufficient capacity of the crossing wires.

Wire Broom Effect on Socket Failure

A socket can include both fully developed crossing wires (wires rupture before slipping) and partially developed crossing wires (wires slip before rupturing). A socket's *wire development ratio* is defined as the fraction of crossing wires that are fully developed. The wire development ratio is therefore a measure of the general tendency for the crossing wires to slip (low ratio) or fracture (high ratio) in a given socket. For the six sockets of known wire broom geometry, the wire development ratio was calculated under the socket's service load and failure load, if applicable (Table 6). The wire development ratio increases with load because the load-induced confinement stress in the casting governs how much friction can be developed between wire and zinc to resist wire slip.

Table 6: Wire development ratio in sockets considered

	Gravity Loads Before M4N Failure						Gravity Loads After M4N Failure	End of Load Test
	M4-4_T	**M8N_T**	**B4S_G**	**B4N_G**	**M4N_T**	**B12W_G**	**M4-4_T**	**B4S_G**
Cable Slip [in]	Unknown	0.625	0.875	0.875	1.125	1.875	Visible	1.375
Wire Development Ratio	58%	43%	47%	60%	59%	38%	65%	66%
Socket Failure Mode	None	None	None	None	Core Rupture	Core Flow-out	Core Rupture	Core Rupture

Four of the six sockets that were analyzed failed or were in the process of failing. The failures of sockets M4N_T and M4-4_T occurred in the field and involved the rupture of multiple outer wires and a significant shift or complete pull-out of the core, which corresponds to core rupture (Figure 48, page 35). The load test of socket B4S_G was stopped after seven outer wires ruptured, indicating that the socket was on the brink of core rupture. Finally, socket B12W_G experienced a very large cable slip as its crossing wires slipped without fracturing, which corresponds to core flow-out (Figure 49 page 35).

The three sockets exhibiting core rupture had a larger wire development ratio (59 to 66 percent) than the socket exhibiting core flow-out (38 percent) (Table 6, Figure 65 right, and Figure 66). This result is consistent with the socket behavior previously introduced (Figure 48 vs. Figure 49, page 35): fully developed wires lead to core fracture, while partially developed wires lead to core flow-out.

Figure 65 summarizes the observed socket behavior: if shear stress is needed on the core surface to resist the full cable tension, the zinc flows and causes cable slip over time. When the cable slip becomes too large, the socket fails in core rupture or core flow-out depending on whether the crossing wires are primarily fully developed or partially developed.

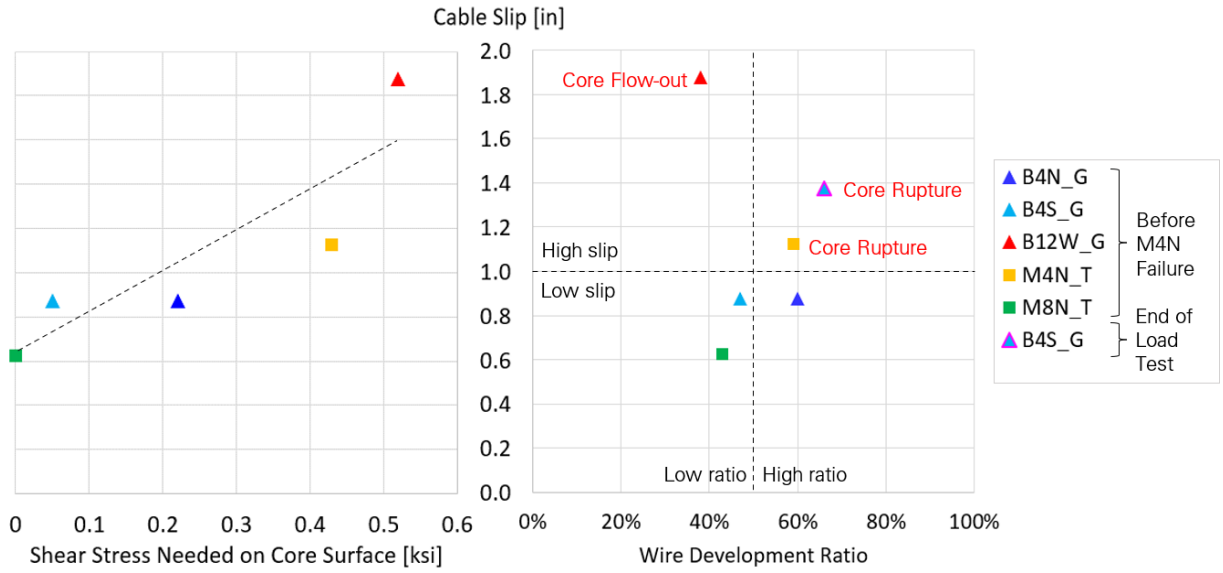

Figure 65: Correlation between core shear stress, wire development ratio, cable slip, and socket failure.

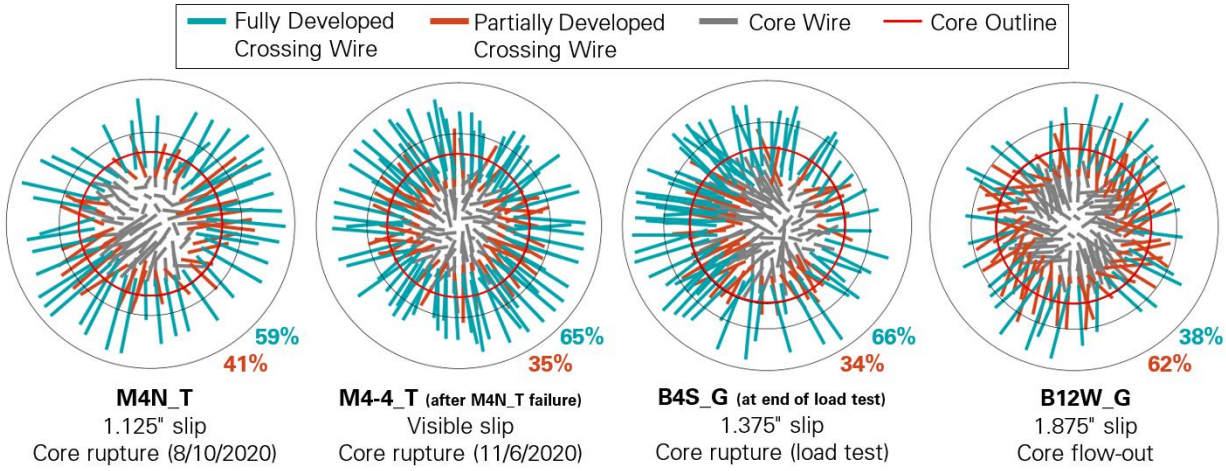

Figure 66: Fully and partially developed crossing wires in failed and failing sockets.

5.0 Discussion

The Arecibo Telescope collapsed after three cables at the top of Tower 4 failed progressively in 2020. It started from the failure of auxiliary main cable M4N on August 10, 2020, followed by the failure of original main cable M4-4 on November 6, 2020, and the failure of original main cable M4-2 on December 1, 2020, which immediately triggered failure of M4-1 and M4-3, allowing the platform to fall. The first three cable failures all occurred within the cable-socket assemblies at Tower 4 and involved the rupture of outer wires inside the socket and a significant deformation or complete pull-out of part of the socket's zinc casting. These failures are therefore referred to herein as *socket failures*.

The degradation of the cable wires over their 57-year life span did not contribute to the socket failures. Issues relating to paint conditions, infrequent cable vibrations, and the moisture exclusion system were observed occasionally during inspections, some of which were remediated prior to 2020. Local corrosion was observed in some individual wires, but there was no widespread corrosion throughout the cable system. Stress corrosion cracks and pitting were not predominant in the collected wire samples. A total of 22 wire breaks were reported before the first cable failure (not including the breaks that had occurred in the replaced cable B12-3 and at the by-passed splice of cable M8-4). The number of broken wires was less than one percent of the total number of wires in the cable system. All but three of these wire breaks occurred prior to the installation of the Gregorian. No wire breaks were reported in cable M4N prior to failure in 2020. The socket failures must, therefore, be attributed to some other mechanism.

The mechanism of zinc flow as presented in Section 4.2.4 explains a high variation of socket behavior observed among the cable sockets. A total of 78 sockets were installed to anchor the cable ends to their supports, including 54 sockets for the original cables and 24 sockets for the auxiliary cables. Prior to the first cable failure, eight auxiliary cable sockets, which is one-third of the auxiliary cable system, exhibited excessive cable slips larger than one-sixth of the cable diameter under sustained tension in a range of 40 to 50 percent of the cables' Minimum Breaking Strengths. The original cable sockets exhibited less significant cable slip even though they were in service approximately twice as long. When the telescope collapsed, three out of 78 sockets (M4N_T, M4-4_T and M4-2_T) had failed by core rupture after exhibiting cable slips of approximately one inch, and one socket (B12W_G) was failing by core flow-out and exhibited a cable slip of almost two inches. All of the telescope's cables had a similar safety factor (between 1.9 and 2.6) under sustained loads, were connected to sockets of similar internal design, and were socketed with a process that did not significantly change between the 1960s (original cables) and the 1990s (auxiliary cables). Yet, the amount of cable slip and the type of failure mode was different between the sockets. The variation of socket behavior is attributed to the variation of wire brooming.

The sockets were zinc-filled spelter sockets. All of the sockets were fabricated by splaying out the ends of the cable wires to form a broom inside the socket cavity and pouring molten zinc to create a cone-shaped casting in the socket. As the wires were bent and splayed manually during brooming, they were not evenly distributed in the radial and circumferential directions. The wire broom geometry is then unique to each socket. This is evident in the range of brooming ratios observed in the sockets that were examined in the laboratory. The zinc used as filling material between the wires and the socket wall was 99.5 percent pure. Pure zinc is a soft and low-strength metal compared to steel. When highly stressed through shear and compression due to confinement at the front of the socket, the zinc deforms plastically and will exhibit considerable ductility. Zinc also exhibits creep at room temperature, at a rate that follows a power law of the sustained stress. Flow of zinc through plastic deformation and creep can result in large deformations, which were clearly visible in the sockets that were cut open.

The capacity of zinc-filled spelter sockets is dependent upon the total strength of splayed wires in the socket. The model presented in Section 4.2 predicts the failure mechanism of the wires and zinc core within the socket based on the collected data from field assessment and laboratory examination. The socket's *long term capacity* is defined as the maximum force that can be resisted by the socket without relying on shear in the zinc. If a sufficient number of wires are splayed out of the zinc casting core, shear in the zinc is minimal and the long-term socket slip is negligible. But if the number of wires splayed out of the core is insufficient, a cascading mechanism forms between splayed wires and zinc core which results in a limited life span of the socket. The socket life span is a function of rate of zinc flow. Zinc flow increases exponentially with the magnitude of the shear stress around the core. Zinc flow results in a gradual slip of the inner wires out of the socket, increasing the tension in the splayed-out wires until they slip or rupture. This creates a cascading effect, and eventually enough wires will slip or rupture to allow the core and inner wires to pull out of the socket.

This phenomenon occurred in several sockets (M4N_T, M4-4_T, M4-2_T and B12W_G) prior to collapse in 2020. The first socket that failed in August 2020 (M4N_T) had exhibited an excessive cable slip of 1.125 inch at an increased slip rate a year and a half before failing. The second socket (M4-4_T) failed three months later, and the third socket (M4-2_T) failed another three weeks later. B12W_G had exhibited a considerable amount of slip prior to failure. For all these sockets, deformation, craters and/or cracks observed at the back of the socket's zinc casting indicated continued zinc flow at an accelerated rate prior to failure.

The sockets of the telescope were in a state of high sustained stress during their life spans. Therefore, for the flow not to occur, the wire brooming becomes critical. A summary of some of the brooming metrics identified in Appendix O is presented in Table 7. Socket B12W_G has a very low wire development ratio, indicating that many of the wires splayed out of the core slip rather than rupture. Since the wires were not rupturing, there would be no redistribution of wire tensions but slip would continue since the zinc shear stress was high as indicated by the low actual-to-minimum safety factor ratio. Socket M4N_T has a high wire development ratio. Therefore, the outer wires would tend to rupture rather than slip. The rupture of wires would cause an increase in the tension in the remaining wires, increasing the zinc shear stress and accelerating the zinc flow. The process continues until there is insufficient shear strength to retain the core and the plug pulls from the socket. Of the sockets opened in the laboratory, the sockets that did not fail (and were not in the process of failing) had a safety factor of at least 95 percent of the minimum safety factor where no shear stress occurs on the core surface. The other four sockets (M4N_T, B12W_G, M4-4_T after M4N_T failure, and B4S_G in the load test) had a safety factor of less than 95 percent of the minimum (as seen in row 6 of Table 7) and failed by core rupture or by core flow-out. In our analysis of the sockets studied in the laboratory, we estimated that the sockets would not have experienced any large cable slips or have failed if their cables had been designed with a minimum safety factor of 3.0. More data is needed to develop an upper bound of safety factor which will provide essentially an infinite life to the sockets. Additionally, more data is needed to develop a relationship between safety factor, quality of brooming, and service life.

Table 7: Summary of socket properties and behavior

	Gravity Loads Before M4N Failure						Gravity Loads After M4N Failure	End of Load Test
	M4-4_T	**M8N_T**	**B4S_G**	**B4N_G**	**M4N_T**	**B12W_G**	**M4-4_T**	**B4S_G**
Cable Slip [in]	Unknown	0.625	0.875	0.875	1.125	1.875	Visible	1.375
Wire Brooming Ratio[A]	61%	69%	61%	60%	59%	57%	61%	61%
Wire Development Ratio[B]	58%	43%	47%	60%	59%	38%	65%	66%
Min. Cable Safety Factor to Not Need Core Shear	1.8	1.7	2.5	2.4	2.4	3.0	1.8	2.5
Actual Cable Safety Factor	2.0	2.2	2.4	2.3	2.2	2.6	1.6	0.98
Actual/Min. Safety Factor	1.11	1.29	0.96	0.96	0.92	0.87	0.89	0.39
Socket Failure Mode	None	None	None	None	Core Rupture	Core Flow-out	Core Rupture	Core Rupture

[A] Quantifies the width of the wire broom (would be 100% if all wire ends were touching the socket's steel).
[B] Fraction of crossing wires that are fully developed. Quantifies the crossing wire's tendency to rupture vs slip (would be 100% if all crossing wires ruptured before slipping).

In the discussion above, the cable force was assumed constant. While hurricanes and earthquakes increased the cable tensions by no more than 15 percent, the model predicts that the resulting tension from the load fluctuation is large enough to increase the shear demand on the core by 30 percent on socket B12W_G and 60 percent on socket M4N_T (Table 5). Given the high level of shear stress already in the zinc core from sustained gravity load, we expect this stress increase, while transient, may have a significant effect on the life span of these sockets. This is very similar to the prediction of fatigue life of components where the accumulated damage of many cycles needs to be considered. Understanding the effect of the accumulation of damage to the sockets can be further studied by a controlled test program using a sufficient number of samples to accommodate the necessary variables. Until then, using a higher safety factor for the sustained load is a conservative design approach to keep the cable wires at a relatively low state of stress and thus minimize zinc flow.

6.0 Conclusions and Recommendations

The progressive cable failures and eventual collapse of the Arecibo Telescope were caused by a combination of factors that impacted the forces and long-term capacities of zinc-filled spelter sockets. Our investigation identified five key factors, which are summarized in the following. Relevant recommendations to mitigate the risk and consequences of socket failure are also provided.

- The wire broom geometry determines the socket's long-term capacity, which is the force that can be resisted by the socket without relying on shear stress in the zinc. Shear stress causes zinc flow, which can lead to large cable slip and socket failure. The telescope's cables were socketed following typical practice, where the cable wires are splayed manually to form a broom before casting the zinc. Due to the manual brooming process, the long-term socket capacity varied between sockets. Zinc-filled spelter sockets with more consistent long-term capacities could be obtained by specifying and controlling the shape of the wire broom during socketing. Proof-loading the cable by testing over a short period is insufficient to assure the long-term capacity of sockets.

- A sufficient safety factor is required to ensure that the socket force is less than the socket long-term capacity. The telescope's cable system was designed with relatively low safety factors under the structure's own weight. The cables were therefore highly stressed over the entire life of the telescope, and not only during extreme environmental events such as hurricanes and earthquakes. This allowed zinc flow to occur over a long period of time in some of the sockets. While the cable system was designed with safety factors between 2.0 and 2.4 under the structure's own weight, those safety factors were not sufficient to prevent long-term zinc flow in sockets with narrow wire brooms. Our analysis indicates that a safety factor of 3.0 under gravity loads would have been needed to prevent long-term zinc flow in the sockets.

- The hurricanes and earthquakes that regularly impact Puerto Rico increased the cable tensions and further lowered the cable safety factors temporarily. We estimated that the cable tensions increased by up to 15 percent. However, this moderate increase was sufficient to develop or increase the shear stress in some of the sockets' zinc and therefore exacerbate zinc flow. Whether zinc flow can occur rapidly during transient high loads would need further investigation. Until this is better understood, a safety factor of 4.0 should be used for the worst loading condition, even if it is transient.

- It is now clear from our study that excessive cable slip occurs in zinc-filled spelter sockets due to zinc flow and is a sign of upcoming failure through core rupture or core flow-out. Excessive cable slip was observed on the first socket that failed at least a year and a half before failure, but was not identified as an immediate structural concern. Monitoring the cable slip and slip rate is a reasonable method to determine if a socket is failing, and the limit of one-sixth of the cable diameter appears to be a reasonable threshold for slip monitoring based on what was observed on the telescope's sockets. Cable slip can cause the rupture of individual outer wires before complete socket failure. A socket exhibiting outer wire ruptures should therefore be closely inspected and monitored for cable slip. However, monitoring wire ruptures is not sufficient to determine if a socket is failing.

- The first socket failure occurred at the end of an isolated cable (M4N), whose tension could not be redistributed to adjacent cables. Instead, this first failure resulted in a rotation of the platform and tension changes throughout the cable system. Designing cluster cable systems with multiple adjacent cables on each span provides redundancy. In the event of a cable failure, the remaining adjacent cables can sustain the increased load for a period of time, allowing and easing the replacement of the failed cable or cables.

More studies are required to characterize the relationship between cable safety factor, quality of brooming, and socket service life. In the meantime, cables terminated with zinc-filled spelter sockets should be designed with a safety factor of at least 3.0 under gravity loads, and at least 4.0 under transient loading conditions. A safe cable system can still be designed with a lower safety factor, such as the 2.2 safety factor prescribed in ASCE 19. However, in that case, the sockets should be inspected regularly to measure cable slip. A socket should be replaced or bypassed when excessive cable slip indicates that zinc flow continues to occur over time. Limiting the allowable cable slip to one-sixth of the cable diameter is reasonable until further studies are performed.

7.0 Acknowledgments

We would like to thank the staff at the Arecibo Observatory, the University of Central Florida, and the National Science Foundation for their assistance in this investigation. We also would like to thank Cornell University for providing access to the Arecibo Observatory archives in the Rare and Manuscript Collections.